



**CBPF**

Centro Brasileiro  
de Pesquisas Físicas

Coordenação de Formação Científica

Master's thesis

**Charged scalar non-massive  
perturbations and special modes in  
Reissner-Nordström spacetime**

Felipe Sobrero Sorage Marques



**Felipe Sobrero Sorage Marques**

**Charged scalar non-massive perturbations and special  
modes in Reissner-Nordström spacetime**

Dissertation presented to the Graduate Course in Physics at the Centro Brasileiro de Pesquisas Físicas, as a partial requirement for obtaining the Master's Degree in Physics.

Supervisor: Marc Casals

July 17, 2024





MINISTÉRIO DA  
CIÊNCIA, TECNOLOGIA  
E INOVAÇÃO



"CHARGED SCALAR FIELD PERTURBATIONS AND SPECIAL MODES  
IN REISSNER-NORDSTRÖM SPACETIME"

**FELIPE SOBRERO SORAGE MARQUES**

Dissertação de Mestrado em Física apresentada no  
Centro Brasileiro de Pesquisas Físicas do  
Ministério da Ciência Tecnologia e Inovação.  
Fazendo parte da banca examinadora os seguintes  
professores:

Marc Casals - Orientador/CBPF

Documento assinado digitalmente  
**gov.br** MAURICIO RICHARTZ  
Data: 19/07/2024 10:48:07-0300  
Verifique em <https://validar.it.gov.br>

Maurício Richartz - UFABC

Documento assinado digitalmente  
**gov.br** BRUNO GERALDO CARNEIRO DA CUNHA  
Data: 02/12/2024 15:34:16-0300  
Verifique em <https://validar.it.gov.br>

Bruno Geraldo Carneiro da Cunha – UFPE

Rio de Janeiro, 17 de julho de 2024.



Dedico essa dissertação a minha família, meus pais Alessandro e Elizabeth, meus irmãos Fernando e Felipe Leandro e meus avós Edson e Luzney, pelo apoio incondicional e inesgotável incentivo. Sem vocês isso jamais seria possível. Muito obrigado.



# Acknowledgements

Aos meus pais, por todos os esforços e incentivos que me permitiram sempre me manter nessa caminhada sendo um apoio incondicional e um exemplo inabalável. Meus avós incansavelmente preocupados, sempre diretamente envolvidos em cada passo que eu dou. Meus primos e padrinhos, Vanderson e Iverson, sempre com extrema atenciosidade em qualquer momento. À minha prima Gabrielle, sempre me ajudando quando preciso. Ao meus melhores amigos e irmãos que estiveram comigo em todos os momentos da minha vida. Os mais difíceis, os mais felizes e, inclusive, no exato segundo em que soube que estudaria na UERJ e agora aqui no CBPF, Felipe Leandro e Fernando. Vocês foram verdadeiramente uma inspiração, amo vocês.

Ao meu orientador Marc Casals, por toda ajuda, pela compreensão e toda a presença sempre que precisei de ajuda, por ter acreditado em mim e me guiado por tantos anos anos.

Aos professores que ministraram os cursos que fiz durante meu mestrado o professor Helayël, professor Ivan, professor Felipe Tovar e o professor Nami. Aos professores do Instituto de Física da UERJ que foram extremamente importantes para minha formação, em especial o professor Henrique, o professor Daniel Barci, o professor Capri e Bruno Alho também.

Aos funcionários do CBPF e da UERJ de forma geral, sempre se esforçando para manter o ambiente que foi, para mim e para tantos amigos, uma segunda casa o mais agradável possível mesmo nos momentos mais difíceis que houveram.

Aos valiosos membros do “grupo secreto”, Allan, Alan e Rebello, amigos que compartilhei tantos momentos felizes e tristes nessa jornada.

Ao meu grande amigo Gabriel (ou Gabi/Gabori), impossível desanimar tendo um exemplo de resiliência como você! Aos meus parceiros de todas as horas Eduardo Valadão e Isaque Porto, comparsas na vida e nos trabalhos sempre! E à minha grande amiga Malu pelo apoio sempre que necessário.

Aos amados “Migos”, amigos tão valiosos que fiz aqui no CBPF: Joaquim, Laís, Luiza, Gabriel, Alan, Edine, JP e Mari! Em especial à você Laís, sem você tudo teria sido impossível nessa reta final! Muito obrigado minha amiga.

Finalmente à eterna Távola: meus amigos e irmãos, Patrick e Alani, sempre estando presentes quando mais preciso de um refúgio. E meu afilhado Vinicius que está distante mas sempre por perto!

E também à todas as pessoas que contribuem, seja através de serviços ou pelos

impostos, garantindo assim que eu e outros como eu possamos nos formar e trabalhar com tanta qualidade.

*“There is a right and a wrong in the Universe  
and the distinction should not be hard to make.*

Mark Waid



# Abstract

Essa tese trata de teoria de perturbações lineares em um buraco negro de Reissner-Nordström. Investigamos um campo escalar carregado e sem massa nos limites quase-extremo e extremo usando frequências puramente reais e complexas. Revisitamos soluções analíticas bem conhecidas do campo no regime quase-extremo, construímos outras soluções para os casos quase-extremo e extremo, e utilizamos soluções numéricas e exatas para comparar nossos resultados e obter uma compreensão mais profunda.

Para frequências reais, construímos, usando essas soluções, o fator de amplificação superradiante nos limites quase-extremo e extremo. Conseguimos demonstrar a descontinuidade que ocorre no limite extremo, para alguns modos, quando temos a frequência de limite superradiante  $\omega_{\text{SR}}$ .

E para frequências complexas, obtivemos modos quase-normais calculando-os com o uso de funções de Heun confluyente aplicando o que chamamos de método de Fiziev. Conseguimos obter um espectro para modos totalmente refletidos. Também investigamos a formação de um *branch cut* em  $\omega = \omega_{\text{SR}}$  quando o buraco negro se torna extremo, assim como o *branch cut* na origem.

Usando esses modos especiais, pudemos estudar a função Green para um buraco negro quase-extremo. Os modos quase-normais, que se tornarão polos, e o *branch cut* na origem, que resultará em uma *power-law tail* para tempos tardios.

**Palavras-chave:** Relatividade Geral, Buracos negros carregados, Equação de Klein-Gordon, Superradiância, Teoria perturbativa, Modos quase-normais.



# Abstract

This thesis focuses on the linear perturbation theory of the Reissner-Nordström black hole. We investigate a charged, massless scalar field using both purely real and complex frequencies in the near-extremal and extremal limits.

We begin by revisiting well-known analytical field solutions in the near-extremal regime and construct additional solutions for both near-extremal and extremal cases. We utilize numerical and exact solutions to compare our results and gain further insights.

For real frequencies, we derive the superradiant amplification factor in the near-extremal and extremal limits using these solutions. We demonstrate the discontinuity that arises in the extremal limit for the superradiant-bound frequency  $\omega_{\text{SR}}$  and the emergence of infinite wiggles.

In the realm of complex frequencies, we calculate quasinormal modes (QNMs) numerically using the confluent Heun function with the methodology referred to as Fiziev's method. Additionally, we analytically determine a spectrum for quasinormal and totally reflected modes around  $\omega \sim \omega_{\text{SR}}$ , confirming well-established results and discovering new ones. Furthermore, we investigate the formation of a branch cut at  $\omega = \omega_{\text{SR}}$  as the black hole approaches extremality, as well as a branch cut at the origin for  $\omega = 0$ .

Utilizing these special modes, we explore the Green function for a near-extremal black hole. The quasinormal modes serve as poles, while the branch cut at the origin contributes to a power-law tail in the late-time behavior.

**Keywords:** General Relativity, Charged black hole, Klein-Gordon equation, Superradiance, Perturbation theory, Quasinormal modes.



# Contents

	<b>Resumo</b> . . . . .	<b>11</b>
	<b>Abstract</b> . . . . .	<b>13</b>
<b>1</b>	<b>INTRODUCTION</b> . . . . .	<b>19</b>
<b>2</b>	<b>REISSNER-NORDSTRÖM BLACK HOLES: CHARGED SPHERI- CALLY SYMMETRIC METRIC</b> . . . . .	<b>21</b>
<b>3</b>	<b>LINEAR PERTURBATIONS</b> . . . . .	<b>23</b>
<b>3.1</b>	<b>Klein-Gordon equation</b> . . . . .	<b>23</b>
3.1.1	Sub-extremal: $Q < M$ . . . . .	23
3.1.2	Extremal: $Q = M$ . . . . .	24
<b>3.2</b>	<b>Physical properties: spectroscopy of charged black holes</b> . . . . .	<b>25</b>
3.2.1	Superradiance . . . . .	25
3.2.1.1	Bosonic field: . . . . .	26
3.2.2	Quasinormal modes . . . . .	26
3.2.3	Totally reflected modes . . . . .	27
3.2.4	Branch cuts . . . . .	27
<b>4</b>	<b>GREEN FUNCTION</b> . . . . .	<b>29</b>
<b>4.1</b>	<b>Quasinormal mode sum</b> . . . . .	<b>31</b>
<b>4.2</b>	<b>Branch cut</b> . . . . .	<b>31</b>
<b>4.3</b>	<b>Motion of a charged massive particle</b> . . . . .	<b>32</b>
4.3.1	Circular orbits . . . . .	33
4.3.2	Zero angular momentum observers . . . . .	34
<b>5</b>	<b>ANALYTICAL SOLUTIONS</b> . . . . .	<b>39</b>
<b>5.1</b>	<b>Sub-extremal solutions: <math>Q &lt; M</math></b> . . . . .	<b>39</b>
5.1.1	Solution valid for quasinormal modes . . . . .	39
5.1.1.1	Near event horizon solution ( $x \ll 1$ ) . . . . .	39
5.1.1.2	Far region ( $x \gg \max(\tau, \varpi)$ ): . . . . .	40
5.1.1.3	Matching ( $\max(\tau, \varpi) \ll x \ll 1$ ): . . . . .	41
5.1.2	Solution valid for branch point . . . . .	41
5.1.2.1	Near event horizon ( $\hat{\omega}x \ll \varpi$ ): . . . . .	41
5.1.2.2	Far region ( $x \gg \max(\tau, \varpi)$ ): . . . . .	42
5.1.2.3	Matching ( $\varpi \ll x \ll \varpi/\hat{\omega}$ ): . . . . .	42

<b>5.2</b>	<b>Extremal solutions: <math>Q = M</math></b>	<b>43</b>
5.2.1	Solution valid for superradiant bound frequencies	43
5.2.1.1	Near event horizon solution ( $x \ll 1/ \beta $ ):	43
5.2.1.2	Far region ( $x \gg  \alpha\beta $ ):	44
5.2.1.3	Matching ( $ \alpha\beta  \ll x \ll  \beta ^{-1}$ ):	44
<b>5.3</b>	<b>Quasinormal frequencies spectrum</b>	<b>44</b>
<b>5.4</b>	<b>Totally reflected frequencies spectrum</b>	<b>46</b>
<b>6</b>	<b>NUMERICAL SOLUTIONS</b>	<b>49</b>
<b>6.1</b>	<b>Sub-extremal solutions: <math>Q &lt; M</math></b>	<b>49</b>
6.1.1	IN-modes solutions	49
6.1.1.1	Comparing solutions:	51
6.1.2	UP-modes solutions	52
6.1.2.1	Comparing solutions:	53
<b>6.2</b>	<b>Extremal solutions: <math>Q = M</math></b>	<b>54</b>
6.2.1	IN-modes solutions	54
6.2.2	UP-modes solutions	54
<b>7</b>	<b>RESULTS</b>	<b>55</b>
<b>7.1</b>	<b>Spectroscopy analysis</b>	<b>55</b>
7.1.1	Superradiance	55
7.1.2	Modes in near-extremal Reissner-Nordström	56
7.1.2.1	Quasinormal modes properties:	57
7.1.2.2	Totally reflected modes properties:	58
7.1.3	Branch cuts	59
<b>7.2</b>	<b>Green Function analysis</b>	<b>61</b>
7.2.1	Numerical	65
7.2.2	Quasinormal modes	66
7.2.3	Branch-cut	69
7.2.4	Retarded Green function	71
<b>8</b>	<b>CONCLUSION</b>	<b>73</b>
	<b>BIBLIOGRAPHY</b>	<b>75</b>

# List of Figures

Figure 1 – Contour to integrate the GF . . . . .	30
Figure 2 – LogLog-plots of real and imaginary parts of $R^{(\text{in})}$ being black and red ones numerical, blue and orange analytical solutions. We are using $qM = 1$ , $\ell = 0$ and $\omega M = \omega_{\text{SR}}M + 0.001$ . . . . .	52
Figure 3 – LogLog-plots of real and imaginary parts of $R^{(\text{up})}$ being black and red ones numerical, blue and orange analytical solutions. We are using $qM = 1$ , $\ell = 0$ and $\omega M = \omega_{\text{SR}}M + 0.001$ . . . . .	53
Figure 4 – Amplification factor $Z_{0\omega}$ (in percentage form) as a function of the frequency with $qQ = 0.999$ . The red dashed curve is the approximation in subsection 5.1.1. . . . .	55
Figure 5 – Plots of $Z_{\ell\omega}$ for $Q = M$ , $qQ = 1$ . The black lines are numerical solutions while dashed red ones using $A_{\ell\omega}^{(\text{in})}$ defined in (5.34). In the left we zoomed very close the superradiant-bound limit from left and from right to show the infinity oscillations, analytically it can also be seen in equation (7.2). . . . .	56
Figure 6 – Amplification factor $Z_{0\omega}$ as a function of the frequency for different values of $Q$ and $qM = 10$ . For $Q < M$ we are considering the $A_{\ell\omega}^{(\text{in})}$ defined in (5.13) and when $Q = M$ the $A_{\ell\omega}^{(\text{in})}$ defined in (5.34). . . . .	56
Figure 7 – Plots of (6.16) for $Q = 0.999M$ , $q = 2/M$ , $\ell = 3$ and $z_\infty = 20$ . We use a contour plot where the red dots are the QNMs on the left and a 3D plot on the right. For these values of charges, $M\omega_{\text{SR}} \simeq 1.91249$ the QNMs with real part close to this value are ZDMs while the other 3 are DMs. . . . .	58
Figure 8 – Plots of $\log_{10}  \mathcal{W} $ for $qM = 10$ . We are using $A_{\ell\omega}^{(\text{in})}$ defined in (5.13). The mode is $\ell = 2$ , and $M\omega_{\text{SR}} \sim 9.56246$ and $9.68866$ . The red dots are the QNMs. . . . .	59
Figure 9 – Plots of $ \mathcal{W} $ as function of a phase $\phi$ (left) and a contour plot of $\log_{10}  \mathcal{W} $ for $Q = M$ , $qQ = 10$ and $\ell = 2$ . We are using $A_{\ell\omega}^{(\text{in})}$ defined in (5.34), the red dot at the center of the contour plot is $\omega = \omega_{\text{SR}}$ . . . . .	59
Figure 10 – Plots of $\log_{10}  \mathcal{W} $ for $qM = 10$ . We are using $A_{\ell\omega}^{(\text{in})}$ defined in (5.13) and (5.34) for $Q < M$ and $Q = M$ , respectively. The mode is $\ell = 4$ , and $M\omega_{\text{SR}} \simeq 9.56246$ , $9.68866$ and $M\omega_{\text{SR}} = 10$ for the respective values of $Q$ . . . . .	60
Figure 11 – Plots of $ \mathcal{W} $ as function of a phase $\phi$ (left) and a contour plot of $\log_{10}  \mathcal{W} $ for $Q = 0.999M$ , $qQ = 9.99$ and $\ell = 2$ . We are using $A_{\ell\omega}^{(\text{in})}$ defined in (5.24), the red dot at the center of the contour plot is $\omega = 0$ . . . . .	60

Figure 12 – Log-plots of the real and imaginary parts of $\mathcal{W}_{\ell\omega}$ for different values of $\ell$ defined using analytical and numerical solutions. Black and red are numerical solutions, while blue and orange the analytical ones, being black/blue real and red/orange imaginary parts around the SR-frequency.	62
Figure 13 – Log-plots of the real and imaginary parts of $f_{\ell\omega}^{(\text{in})} f_{\ell\omega}^{(\text{up})}$ for different values of $\ell$ defined using analytical and numerical solutions. Black and red are numerical solutions, while blue and orange the analytical ones, being black/blue real and red/orange imaginary parts.	62
Figure 14 – Plots of the real and imaginary parts of $G_\ell$ for different values of $\ell$ defined using analytical and numerical solutions. Black and red are numerical solutions, while blue and orange the analytical ones, being black/blue real and red/orange imaginary parts.	63
Figure 15 – Log-plots of the real and imaginary parts of $\mathcal{W}_{\ell\omega}$ for different values of $\ell$ defined using analytical and numerical solutions. Black and red are numerical solutions, while blue and orange the analytical ones, being black/blue real and red/orange imaginary parts for low-frequencies.	63
Figure 16 – Log-plots of the real and imaginary parts of $f_{\ell\omega}^{(\text{in})} f_{\ell\omega}^{(\text{up})}$ for different values of $\ell$ defined using analytical and numerical solutions, in the approximation of low-frequencies. Black and red are numerical solutions, while blue and orange the analytical ones, being black/blue real and red/orange imaginary parts.	64
Figure 17 – Plots of the real and imaginary parts of $G_\ell$ for different values of $\ell$ defined using analytical and numerical solutions in the approximation of low-frequencies. Black and red are numerical solutions, while blue and orange the analytical ones, being black/blue real and red/orange imaginary parts.	64
Figure 18 – Log-plots of the real (black) and imaginary (red) parts of $G_0$ .	65
Figure 19 – Plot for the real (black) and imaginary (red) parts of $G_0$ .	66
Figure 20 – Log-plot and loglog-plot of real part of $\mathcal{G}_0^{\text{ret}}$ .	66
Figure 21 – Plots of $ C_{\ell,n+1}/C_{\ell,n} $ using $T = \pm 10$ for different values of $\ell$ .	67
Figure 22 – Log-plots of the real part of $G_{\ell,n}^{\text{QN}}$ .	68
Figure 23 – Log-plot and loglog-plot of $\mathcal{G}_0^{\text{QN}}$ .	68
Figure 24 – Log-plot and loglog-plot of numerical $\mathcal{G}_0^{\text{ret}}$ and $\mathcal{G}_0^{\text{QN}}$ for several times.	69
Figure 25 – Log-plot $G$ .	70
Figure 26 – Log-plot $G$ .	70
Figure 27 – Log-plot and loglog-plot of individual modes of $\mathcal{G}_\ell^{\text{QN}}$ .	71
Figure 28 – Loglog-plot of individual modes of $\mathcal{G}_\ell^{\text{BC}}$ .	71
Figure 29 – Loglog-plot of $ \mathcal{G}^{\text{BC}} + \mathcal{G}^{\text{QN}} $ .	72

# 1 Introduction

The General Relativity (GR) is the most acceptable theory to describe gravitational phenomena, but more than describing these phenomena, the change in the very conception of space and time is fundamental to all modern physics. The emergence of black holes (BH) could only be possible having in mind this new notion of space-time and understanding it as being the geometry itself.

The study of BH perturbations starts with Regge & Wheeler [[Regge e Wheeler 1957](#)] in the 1950s. At the end of the 1960s, Penrose discovered that it is possible to extract rotational energy from a rotating BH [[Penrose 1969](#)], and Christodoulou explored this for the first time [[Christodoulou 1970](#)]. This well-known process, known as the Penrose Process, occurs with unstable particles. These particles should get close enough to the BH and "break", letting one part fall into the BH while the other part escapes, resulting in an escaping particle with more energy than the original one. In the early 1970s, Zel'dovich showed that the extraction of energy could also occur with electromagnetic waves in an analogous scenario [[Zel'Dovich 1971](#)]. In his seminal work, he considered the scattering of an electromagnetic wave by a conducting cylinder rotating with a certain angular velocity. For waves with specific frequencies, they have reflected parts with an amplitude exceeding the amplitude of the incident wave. This bound frequency is what we call the superradiant-bound limit. In 1972, Press & Teukolsky finally reproduced these results of Zel'dovich for scalar waves interacting with a Kerr BH [[Press e Teukolsky 1972](#)] and then generalized it for spinorial, electromagnetic, and gravitational waves [[Teukolsky 1973](#), [Press e Teukolsky 1973](#), [Teukolsky e Press 1974](#)], where for scalar, electromagnetic, and gravitational cases this effect (the amplification of the reflected wave) appears and is well-known as Superradiance.

However, it is not an exclusive effect of rotating BH. While a field can extract rotational energy from a BH, a charged field can also extract energy from a charged BH. The effect is the same, but while the superradiance generated by a rotating BH is induced always in the neighborhood of the event horizon, in the ergosphere, for charged interaction the region where energy extraction occurs varies depending on the physical parameters of the field. This will not be addressed here, but a good discussion is developed by Di Menza & Nicolas [[Menza e Nicolas 2015](#)].

In 1983, Chandrasekhar's incredible book [[Chandrasekhar 1998](#)] provided a complete study of perturbation theory of scalar and spinorial fields in RN spacetime (also in Kerr). More recently, Brito, Cardoso & Pani, in yet another amazing book, explored the superradiance phenomenon in a much more modern language [[Brito, Cardoso e Pani 2020](#)].

But more than a very interesting effect by itself, the presence of the superradiance impacts the perturbation fields, in our case the charged scalar ones, in a few ways. Being a dissipative system, special types of modes with complex frequencies exist, assuming a time dependence like  $e^{-i\omega t}$  and with  $\Im\omega < 0$ : damped modes. Some of these damped special modes will describe quasinormal modes (QNMs), and others totally reflected modes (TRMs), and both of them are related to the superradiant-bound limit, as we will see in the next chapters.

These QNMs [[Vishveshwara 1970](#), [Hod 2010](#)] are very important. It is this kind of vibration, when a BH emits gravitational waves, that is detected by the Laser Interferometer Gravitational-Wave Observatory (LIGO) [[Abbott et al. 2016](#)]. And these modes will be the poles of the Wronskian of the field solutions, which play a very important role when we investigate the Green function. All of it will be explored.

In this work, we choose units such that  $G = c = 1$ .

# 2 Reissner-Nordström black holes: charged spherically symmetric metric

The most realistic case for BHs is the rotating BH without an electric charge. However, the Reissner-Nordström (RN) BH serves as a great toy model for reasons that will become clear throughout the thesis. and in the next sections. The RN metric has mass  $M$  and charge  $Q$ , and in the Boyer-Lindquist coordinates, it is described by

$$ds^2 = -\frac{\Delta}{r^2} dt^2 + \frac{r^2}{\Delta} dr^2 + r^2 (d\theta^2 + \sin^2 \theta d\varphi^2), \quad (2.1)$$

where  $\Delta = r^2 - 2Mr + Q^2$ , and the range of coordinates are:  $t \in (-\infty, +\infty)$ ,  $r \in (0, +\infty)$ ,  $\theta \in [0, \pi]$ ,  $\varphi \in [0, 2\pi]$ . The RN metric is obtained by solving the Einstein-Maxwell equation considering an electromagnetic potential  $A_\mu$  with a unique non vanish element  $A_0 = -Q/r$ .

We can see from equation (2.1) that this metric diverges for  $r = 0$  and  $\Delta = 0$ , however checking the Kretschmann scalar it diverges only when  $r = 0$ , which indicates a physical singularity at the origin.

Although, the other two points diverge the metric describing nonphysical singularities at  $r = r_\pm$  where  $r_\pm = M \pm \sqrt{M^2 - Q^2}$ . These two surfaces  $r_+$  is the exterior horizon (the event horizon) and  $r_-$  is the inner horizon.

The first one, the event horizon, is a surface where for  $r < r_+$  any information is inaccessible to an outside observer. It happens because the light cone are deformed so that they point only inwards to the BH.

Considering the weak cosmic censorship hypothesis we need to guarantee the singularity is always surrounded by an event horizon, and looking at  $\Delta = 0$ , it only happens if  $Q \leq M$ . When  $Q$  has this maximum value we call it as extremal RN BH, and  $r_H = r_+ = r_-$ .



# 3 Linear Perturbations

In this section, we will first review the propagation of perturbations of scalar charged waves around RN BH and then examine the physical properties of this field through a type of spectroscopic study.

## 3.1 Klein-Gordon equation

### 3.1.1 Sub-extremal: $Q < M$

A massless charged scalar field  $\Psi$  propagating on a RN spacetime background will be described by a Klein-Gordon (KG) equation,

$$(\nabla^\mu - iqA^\mu)(\nabla_\mu - iqA_\mu)\Psi = 0, \quad (3.1)$$

and we can define the scalar field using an appropriate ansatz as

$$\Psi = \frac{1}{2\pi} \sum_{\ell=0}^{\infty} \sum_{m=-\ell}^{\ell} \int_{-\infty}^{+\infty} R_{\ell\omega}(r) P_\ell(\theta) e^{im\varphi} e^{-i\omega t} d\omega. \quad (3.2)$$

where  $\omega$  is the frequency of the field and  $P_\ell(\theta)$  is the spherical harmonics.

The equation for the radial component of the field,  $R_{\ell\omega}$ , can be described as

$$\frac{d}{dr} \left( \Delta \frac{dR}{dr} \right) + \left( \frac{K^2}{\Delta} - \lambda_\ell \right) R = 0, \quad (3.3)$$

where  $K = \omega r^2 - qQr$  and  $\lambda_\ell = \ell(\ell + 1)$  is a separation constant. And, of course,  $R$  is just a more compact form to write  $R_{\ell\omega}$ .

We can identify two regular singular points at  $r = r_\pm$  and an irregular one at  $r \rightarrow \infty$ . This structure identifies a confluent Heun equation and will be explored further.

Defining  $f_{\ell\omega} = r R_{\ell\omega}$  and using tortoise coordinate  $r_*$ , defined by  $dr_* = r^2/\Delta dr$ , or

$$r_* \equiv \int \frac{dr_*}{dr} dr = r - \frac{r_-^2}{r_+ - r_-} \log \left( \frac{r - r_-}{r_-} \right) + \frac{r_+^2}{r_+ - r_-} \log \left( \frac{r - r_+}{r_+} \right), \quad (3.4)$$

the master equation assumes a Schrödinger-like form

$$\frac{d^2 f}{dr_*^2} + W(r_*) f = 0, \quad (3.5)$$

where

$$W_{\ell\omega} = \frac{\Delta}{r^4} \left\{ \frac{K^2}{\Delta} - \lambda_\ell - \frac{2M}{r} + \frac{2Q^2}{r^2} \right\}. \quad (3.6)$$

We can solve it analytically in the asymptotic regimes and find two linearly independent solutions,  $f_{\ell m\omega}^{\text{in}}$  and  $f_{\ell m\omega}^{\text{up}}$ . These regimes are near the event horizon, when  $r \rightarrow r_+$  (and  $r_* \rightarrow -\infty$ ) and at radial infinity when  $r \rightarrow +\infty$  (and  $r_* \rightarrow +\infty$ ), and will have the following form:

$$f_{\ell\omega}^{(\text{in})} \sim \begin{cases} A_{\ell\omega}^{(\text{out})} r_*^{-iqQ} e^{i\omega r_*} + A_{\ell\omega}^{(\text{in})} r_*^{+iqQ} e^{-i\omega r_*} & , r_* \rightarrow +\infty \\ e^{-i\tilde{\omega} r_*} & , r_* \rightarrow -\infty \end{cases} \quad (3.7)$$

$$f_{\ell\omega}^{(\text{up})} \sim \begin{cases} r_*^{-iqQ} e^{i\omega r_*} & , r_* \rightarrow +\infty \\ B_{\ell\omega}^{(\text{in})} e^{-i\tilde{\omega} r_*} + B_{\ell\omega}^{(\text{out})} e^{i\tilde{\omega} r_*} & , r_* \rightarrow -\infty \end{cases} \quad (3.8)$$

where  $\tilde{\omega} = \omega - \frac{qQ}{r_+}$ .

The physical meanings of these two solutions are different. The IN-modes, described by (3.7), are waves initially propagated from infinity; the wave interacts with the potential barrier  $W_{\ell\omega}$ , that we can see in equation (3.6), being partially reflected back to infinity and partially transmitted into the BH. And the UP-modes, described by (3.8), we have waves propagated near the event horizon, where again, interacting with the potential barrier, are partially reflected back to the BH and partially transmitted to infinity.

Now, using  $f_{\ell\omega}^{(\text{in/up})}$ , we can construct an important quantity: the Wronskian,  $\mathcal{W}_{\ell\omega}$ ,

$$\mathcal{W}_{\ell\omega} \equiv \left( f^{(\text{in})} \frac{df^{(\text{up})}}{dr_*} - f^{(\text{up})} \frac{df^{(\text{in})}}{dr_*} \right) = 2i\omega A_{\ell\omega}^{(\text{in})}. \quad (3.9)$$

### 3.1.2 Extremal: $Q = M$

In this case the equation (3.3) will keep the same shape, but  $\Delta$  now can be written as  $\Delta = (r - M)^2$ ,

$$\frac{d}{dr} \left( (r - M)^2 \frac{dR}{dr} \right) + \left( \frac{K^2}{(r - M)^2} - \lambda_\ell \right) R = 0, \quad (3.10)$$

with  $K = \omega^2 r - qMr$  in this case.

This will change, in a certain way, the structure of the differential equation because from now on we will have only two singular points, at  $r = M$  and  $r \rightarrow +\infty$ , both of them irregular ones. What identifies a doubly-confluent Heun function.

Changing the tortoise coordinate to  $dr_*^{\text{ext}} = (r - M)^{-2} r^2 dr$ , or

$$r_*^{\text{ext}} \equiv \int \frac{dr_*^{\text{ext}}}{dr} dr = r - M - \frac{M^2}{r - M} + 2M \log\left(\frac{r - M}{M}\right), \quad (3.11)$$

we will have the same equation (3.5) with potential (3.6), of course, with  $Q = M$ .

And about the way to write  $r_*^{\text{ext}}$  using (3.11) we choose the right constant with relation to the sub-extremal coordinate (3.4) to have a “smooth transition” when we are increasing the charge and definitely become extremal.

## 3.2 Physical properties: spectroscopy of charged black holes

We will examine some physical properties of spin-field perturbations in two aspects: in the real-frequency domain, investigating the phenomenon of superradiance and exploring the amplification factor; and in the complex-frequency domain, analyzing quasinormal modes (QNMs) and totally reflected modes (TRMs), and their accumulation leading to a branch cut at the superradiant-bound frequency ( $\omega_{\text{SR}}$ ).

None of the phenomena described above are exclusive to RN BH; on the contrary, they apply to other systems, specifically rotating BHs (Kerr spacetime). A charged-scalar field in RN spacetime ends up being “analogous” to a scalar field in Kerr spacetime; or, in other words, it represents a simplified version of the same physical process. This serves as a significant motivator.

### 3.2.1 Superradiance

Superradiance is a phenomenon in which a wave extracts energy from the BH, resulting in an amplification of its reflected part. It is akin to the well-known “Penrose process,” where a small object passing through a region of a rotating BH splits into two parts, with one part entering the BH and the other escaping with greater energy than the original object, thereby decreasing the BH’s spin.

Superradiance can be defined by studying the variation of the energy of the incident ( $E_{\text{in}}$ ) and reflected ( $E_{\text{out}}$ ) parts of the wave coming from infinity,

$${}_s Z_{\ell m \omega} = \frac{dE_{\text{out}}}{dE_{\text{in}}} - 1, \quad (3.12)$$

where  ${}_s Z_{\ell m \omega}$  is the amplification factor.

This quantity quantifies the degree of superradiance. When  $dE_{\text{out}}/dE_{\text{in}} > 1 \therefore dE_{\text{out}}/dt > dE_{\text{in}}/dt$  the wave is extracting energy from BH (the definition of superradiance). This occurs when  $\omega < qQ/r_+$ . Hence,  $\omega_{\text{SR}} \equiv qQ/r_+$  is the superradiant-bound frequency.

### 3.2.1.1 Bosonic field:

For a bosonic field ( $s = 0$ , our case) we can relate the energy fluxes with the amplitudes in (3.9),

$$\frac{d^2 E}{dt d\Omega} = \lim_{r \rightarrow +\infty} r^2 T^r_t, \quad (3.13)$$

which gives us

$$\frac{dE_{\text{out}}}{dt} = \frac{\omega^2}{2} |\mathcal{R}|^2, \quad \frac{dE_{\text{in}}}{dt} = \frac{\omega^2}{2}. \quad (3.14)$$

These quantities  $\mathcal{R}$  and  $\mathcal{T}$  will be defined using the Wronskian between  $f_{\ell\omega}$  and  $f_{\ell\omega}^*$ , helping us understand  $\omega_{\text{SR}}$ . From this, we obtain the following equation

$$|\mathcal{R}|^2 = 1 - \left(1 - \frac{qQ}{\omega r_+}\right) |\mathcal{T}|^2, \quad (3.15)$$

where  $\mathcal{R} = A^{(\text{out})}/A^{(\text{in})}$  and  $\mathcal{T} = 1/A^{\text{in}}$ , representing the reflection and transmission coefficients, respectively. Here, we denote  $A^{(\text{in/out})} = A_{\ell\omega}^{(\text{in/out})}$  for simplicity.

Equation (3.15) indicates that superradiant scattering occurs ( $|\mathcal{R}|^2 > 1$ ) whenever  $\omega < qQ/r_+$ . The amplification factor is defined, in this case, as

$$Z_{\ell m \omega} = |\mathcal{R}|^2 - 1. \quad (3.16)$$

## 3.2.2 Quasinormal modes

The previous section only discussed real frequencies. Now, we are interested in complex ones, particularly quasinormal modes (QNMs), which are crucial in the context of BHs.

According to the uniqueness [Israel 1967, Israel 1968] and no-hair theorem [Ruffini e Wheeler 1971], a BH in a stable configuration is characterized by three (potential) parameters: mass  $M$ , charge  $Q$  and angular momentum  $J$ . QNMs, on the other hand, are characterized (potentially) by a mass parameter  $\mu$ , a charge parameter  $q$ , an orbital number  $\ell$ , an azimuthal number  $m$ , and a spin parameter  $s$ .

QNMs are field modes that decay exponentially with time. They are described by a purely out-going wave at infinity and an in-going wave into the event horizon, leading to a change in the boundary condition,

$$f_{\ell\omega\ell n} \sim \begin{cases} A_{\ell\omega\ell n}^{(\text{out})} r_*^{-iqQ} e^{i\omega\ell n r_*} & , r_* \rightarrow +\infty \\ e^{-i\tilde{\omega}\ell n r} & , r_* \rightarrow -\infty \end{cases} \quad (3.17)$$

where  $\omega_{\ell n}$  is a quasinormal (QN) frequency.

As QNMs represent dissipating fields, they have negative imaginary parts in their frequencies, indicating damping with time. These frequencies are countable but infinite for each set of multipole numbers  $\ell$  enumerated by  $n = 0, 1, 2, \dots$ , with  $n$  representing the fundamental mode with the smallest imaginary value, or in other words, the longest-lived mode.

### 3.2.3 Totally reflected modes

In addition to QNMs, we have another set of modes important in the BH context, also characterized by the same set of parameters as QNMs. These modes, known as totally reflected modes (TRMs), correspond to waves with no transmission,  $\mathcal{T} = 0$ . Like QNMs, they form a countable but infinite spectrum for each set of multipole  $\ell$  enumerated by  $n = 0, 1, 2, \dots$ , we will denote this spectrum as  $\bar{\omega}_{\ell n}$ .

Therefore,  $\mathcal{T} = 0$  implies that  $A_{\ell\bar{\omega}_n}^{(\text{in})} \rightarrow \infty$ . Moreover, it will be useful to consider the absolute value of the Wronskian to find these frequencies.

In summary, the behavior of the Wronskian can be defined as

$$|\mathcal{W}_{\ell\omega}| = \begin{cases} 0 & , \omega = \omega_{\ell n} \\ \infty & , \omega = \bar{\omega}_{\ell n} \end{cases} \quad (3.18)$$

### 3.2.4 Branch cuts

In sub-extremal or extremal cases is well-known presence of a branch point at  $\omega = 0$  due to the irregular character of the singularity of the radial ODE (3.3) at  $r \rightarrow \infty$ , and forming a branch cut (BC) at  $\omega = 0 - i\nu$ , where  $\nu \in [0, +\infty)$ . Physically, the contribution to the field is the late times' decay.

However, in the extremal case (as will become more evident later), another branch point appears at  $\omega = \omega_{\text{SR}}$ , forming a BC at  $\omega = \omega_{\text{SR}} - i\nu$ , where  $\nu \in [0, +\infty)$ . This BC is formed due to a succession of QNMs and TRMs, as will be demonstrated later.



## 4 Green function

The Green function (GF) is a fundamental mathematical object in physics, both classical and quantum. In the context of BHs, it plays a crucial role and can be employed to determine significant quantities such as the self-field and self-force of a field [Casals et al. 2013].

In our study, we focus on a charged scalar particle following a circular trajectory (non-geodesic due to the Lorentz force), and nearly all the quantities described in the previous sections are essential for constructing the GF.

To begin, employing a multipole- $\ell$  decomposition in the angular distance  $\gamma$ , the GF can be expressed as:

$$G_{\text{ret}}(x, x') = \sum_{\ell=0}^{\infty} \mathcal{G}_{\ell}^{\text{ret}}, \quad (4.1)$$

$$\mathcal{G}_{\ell}^{\text{ret}} = \frac{1}{rr'} (2\ell + 1) P_{\ell}(\cos \gamma) G_{\ell}^{\text{ret}}(r, r', \Delta t), \quad (4.2)$$

where  $r$  and  $t$  are the radial and time coordinates of spacetime point  $x$ , respectively, and  $r'$  and  $t'$  are those of spacetime point  $x'$ . Here,  $\Delta t \equiv t - t'$ , and  $\cos \gamma = \cos \theta \cos \theta' + \sin \theta \sin \theta' \cos(\varphi - \varphi')$ .

The Fourier-mode decomposition in time yields:

$$G_{\ell}^{\text{ret}}(r, r', \Delta t) = \frac{1}{2\pi} \int_{-\infty+ic}^{+\infty+ic} d\omega G_{\ell}(r, r', \omega) e^{-i\omega \Delta t}, \quad (4.3)$$

where  $c > 0$ .

The retarded GF satisfies the wave equation (3.5):

$$\left[ \frac{d^2}{dr_*^2} + W_{\ell\omega}(r) \right] G_{\ell}(r, r', \omega) = -\delta(r_* - r'_*), \quad (4.4)$$

where  $W_{\ell\omega}$  is defined in (3.6), and  $K$  is defined in (3.3).

The solution of Fourier-modes of the GF is given by:

$$G_{\ell}(r, r', \omega) = -\frac{f^{(\text{in})}(r_{<}, \omega) f^{(\text{up})}(r_{>}, \omega)}{\mathcal{W}(\omega)}, \quad (4.5)$$

where  $r_{>} \equiv \max(r, r')$  and  $r_{<} \equiv \min(r, r')$ , and  $f^{(\text{in/up})}(r, \omega) \equiv f_{\ell\omega}^{(\text{in/up})}(r)$ .

This allows us to perform an analytical extension and choose an appropriate contour, as illustrated in Figure 1, for integration.

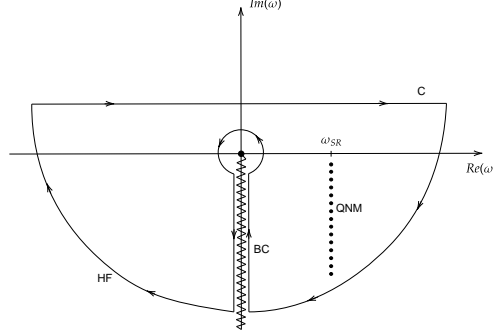


Figure 1 – Contour to integrate the GF

Various contributions can be identified when attempting to integrate it. We have simple poles that will appear from zeros of the Wronskian (QNMs), as explained in subsection 3.2.2. We have a branch cut ( $\Re\omega = 0$ ) in the negative imaginary axis, as explained in subsection 3.2.4, and a high-frequency (HF) arc (which reduces to the flat-space GF when  $M, Q \rightarrow 0$ ).

In other words, we have

$$\begin{aligned} \frac{1}{2\pi} \oint_C d\omega G_\ell(r, r', \omega) e^{-i\omega\Delta t} &= \frac{1}{2\pi} \int_{-\infty+ic}^{+\infty+ic} d\omega G_\ell(r, r', \omega) e^{-i\omega\Delta t} \\ &+ \frac{1}{2\pi} \int_{\text{HF}} d\omega G_\ell(r, r', \omega) e^{-i\omega\Delta t} \\ &+ \frac{1}{2\pi} \int_{\text{BC}} d\omega G_\ell(r, r', \omega) e^{-i\omega\Delta t} \end{aligned} \quad (4.6)$$

the left side of this expression is also equal to the sum of the residues of  $G_\ell$ ,

$$\frac{1}{2\pi} \oint_C d\omega G_\ell(r, r', \omega) e^{-i\omega\Delta t} = i \sum_n \lim_{\omega \rightarrow \omega_n} (\omega - \omega_n) G_\ell(r, r', \omega) e^{-i\omega\Delta t} \equiv G_\ell^{\text{QN}}. \quad (4.7)$$

Therefore, we can write:

$$G_\ell^{\text{ret}} = G_\ell^{\text{QN}} + G_\ell^{\text{BC}} + G_\ell^{\text{HF}}, \quad (4.8)$$

the last one,  $G_\ell^{\text{HF}}$  will not be explored in this work.

## 4.1 Quasinormal mode sum

As discussed earlier, QNMs are defined as complex frequencies where  $\mathcal{W}(\omega_{\ell n}) = 0$ , describing a simple pole in the Fourier mode of the GF. This contribution can be expressed as:

$$G_\ell^{\text{QN}} = - \sum_{n=0}^{\infty} \lim_{\omega \rightarrow \omega_{\ell n}} (\omega - \omega_{\ell n}) \frac{f^{(\text{in})}(r, \omega) f^{(\text{up})}(r', \omega)}{2\omega A_{\ell\omega}^{(\text{in})}} e^{-i\omega\Delta t} \quad (4.9)$$

Thus, the integral (4.3) for  $G_\ell^{\text{QN}}$  becomes, upon solving the limit:

$$G_\ell^{\text{QN}}(r, r', \Delta t) = - \sum_{n=0}^{\infty} G_{\ell,n}^{\text{QN}}(r, r', \Delta t) \quad (4.10)$$

$$G_{\ell,n}^{\text{QN}}(r, r', \Delta t) = \frac{f_\ell^{\text{in}}(r, \omega_{\ell n}) f_\ell^{\text{up}}(r', \omega_{\ell n})}{2\omega_{\ell n} \alpha_{\ell n}} e^{-i\omega_{\ell n} \Delta t}, \quad (4.11)$$

where  $A_{\ell,n}^{(\text{in/out})} \equiv A_{\ell\omega=\omega_{\ell n}}^{(\text{in/out})}$ , and  $\alpha_{\ell n}$  is defined using  $A_{\ell\omega}^{(\text{in})} \sim (\omega - \omega_{\ell n})\alpha_{\ell n}$  when  $\omega \rightarrow \omega_{\ell n}$ .

## 4.2 Branch cut

The BC integral  $G_\ell^{\text{BC}}$ , is defined as

$$\int_{\text{BC}} d\omega G_\ell(r, r', \omega) e^{-i\omega\Delta t} = \int_{L_\uparrow} d\omega G_\ell(\omega + \epsilon) e^{-i\omega\Delta t} + \int_{L_\downarrow} d\omega G_\ell(\omega - \epsilon) e^{-i\omega\Delta t}, \quad (4.12)$$

Let's examine each term separately. In  $L_\uparrow$  the integration range is  $(-iR, 0)$  where  $\omega = \nu e^{-i\pi/2} \equiv -i\nu$ , Making this variable change and using the limit  $R \rightarrow \infty$  we get,

$$\int_{L_\uparrow} d\omega G_\ell(\omega + \epsilon) e^{-i\omega\Delta t} = i \int_0^\infty d\nu G_\ell(-i\nu + \epsilon) e^{-\nu\Delta t}, \quad (4.13)$$

similarly, in  $L_\downarrow$  the integration range is  $(0, -iR)$  where  $\omega = -i\nu e^{2i\pi}$ . Thus, we have:

$$\int_{L_\downarrow} d\omega G_\ell(\omega - \epsilon) e^{-i\omega\Delta t} = -i \int_0^\infty d\nu G_\ell(-i\nu - \epsilon) e^{-\nu\Delta t}, \quad (4.14)$$

consequently, we obtain:

$$\int_{\text{BC}} d\omega G_\ell(r, r', \omega) e^{-i\omega\Delta t} = i \int_0^\infty d\nu \Delta G_\ell(r, r', \nu) e^{-\nu\Delta t}, \quad (4.15)$$

where

$$\Delta G_\ell(r, r', \nu) = G_\ell(-i\nu + \epsilon) - G_\ell(-i\nu - \epsilon). \quad (4.16)$$

And finally we have:

$$G_\ell^{\text{BC}}(r, r', \Delta t) = -\frac{i}{2\pi} \int_0^\infty \Delta G_\ell(r, r', \nu) e^{-\nu \Delta t} d\nu, \quad (4.17)$$

As defined in equation (4.5), we have:

$$\Delta G_\ell(r, r', \nu) = -\frac{f^{(\text{in})}(r, \epsilon - i\nu) f^{(\text{up})}(r', \epsilon - i\nu)}{2\nu A_\ell^{(\text{in})}_{\epsilon - i\nu}} + \frac{f^{(\text{in})}(r, -\epsilon - i\nu) f^{(\text{up})}(r', -\epsilon - i\nu)}{2\nu A_\ell^{(\text{in})}_{-\epsilon - i\nu}}, \quad (4.18)$$

looking further ahead in subsection 5.1.2, it's easy to note that  $f^{(\text{in})}$  don't "feel" the BC because it's not a multi-valuated function, as evident from its definition in equation (5.17). The same doesn't apply to  $f^{(\text{up})}$  or  $A^{(\text{in})}$ , defined respectively in equations (5.18) and (5.24). Terms like  $\omega^{1/2}$  will yield different results considering  $\omega = -i\nu$  or  $\omega = -i\nu e^{2i\pi}$ .

Therefore, equation (4.18) can be written as:

$$\Delta G_\ell(r, r', \nu) = -\frac{f^{(\text{in})}(r, -i\nu)}{2\nu} \left[ \frac{f^{(\text{up})}(r', \epsilon - i\nu)}{A_\ell^{(\text{in})}_{\epsilon - i\nu}} - \frac{f^{(\text{up})}(r', -\epsilon - i\nu)}{A_\ell^{(\text{in})}_{-\epsilon - i\nu}} \right] \quad (4.19)$$

and as we already explained, the term  $\epsilon - i\nu$  is the same as  $-i\nu e^{i0}$  while  $-\epsilon - i\nu$  is  $-i\nu e^{2\pi i}$ .

### 4.3 Motion of a charged massive particle

To calculate the orbits, we first define the Lagrangian of the system:

$$\mathcal{L} = \frac{1}{2} g_{\mu\nu} \dot{x}^\mu \dot{x}^\nu + \frac{q}{\mu} A_\mu \dot{x}^\mu, \quad (4.20)$$

where the 4-velocity of a massive particle is normalized as:

$$-1 = g_{\mu\nu} \dot{x}^\mu \dot{x}^\nu. \quad (4.21)$$

Utilizing the canonical momentum for the coordinates  $t$  and  $\varphi$ , we obtain two conserved quantities:

$$\frac{E}{\mu} = \frac{\Delta}{r^2} \dot{t} + \frac{qQ}{\mu r} \quad (4.22)$$

$$\frac{h}{\mu} = r^2 \sin^2 \theta \dot{\varphi}, \quad (4.23)$$

where  $E$  and  $h$  represent the energy and angular momentum of the particle, respectively, as measured by an observer at infinity. The spherical symmetry in the RN spacetime enables us to translate any movement to the equatorial plane without loss of generality, so we fix  $\theta = \pi/2$ . By combining equations (4.22) and (4.23) into (4.21), we derive the balance of energy:

$$\dot{r}^2 + \frac{\Delta}{r^2} \left( 1 + \frac{h^2}{\mu^2 r^2} \right) = \frac{1}{\mu^2} \left( E - \frac{qQ}{r} \right)^2. \quad (4.24)$$

We can define the value of  $E/\mu$  when the radial kinetic energy of the particle vanishes,

$$V_{\pm} \equiv \frac{E^{\pm}}{\mu} = \frac{qQ}{\mu r} \pm \sqrt{\frac{\Delta}{r^2} \left( 1 + \frac{h^2}{\mu^2 r^2} \right)} \quad (4.25)$$

where the effective potential with positive or negative signs correspond to a solution with

$$\lim_{r \rightarrow +\infty} E^{\pm} = \pm\mu, \quad (4.26)$$

it's notable that:

$$E^+(h, q, r) = -E^-(h, -q, r) \quad (4.27)$$

and this potential greatly depends on the sign of  $qQ$ . For instance,  $E^+ < 0$  when  $qQ < 0$ .

### 4.3.1 Circular orbits

To compare with well-known results in the literature [Pugliese, Quevedo e Ruffini 2011, Pugliese, Quevedo e Ruffini 2011], we choose  $V_+$  for the potential.

Circular orbits will be founded investigating the critical point of the potential, Thus, we have the condition defined in equation (4.25) and

$$\frac{dV_+}{dr} = 0, \quad (4.28)$$

which, when solved, yields a condition for the angular momentum:

$$\frac{(h^{\pm})^2}{\mu^2} = \frac{r^2}{2\Sigma^2} \left[ 2(Mr - Q^2)\Sigma + \frac{q^2 Q^2}{\mu^2} \Delta \pm Q\Delta \sqrt{\frac{q^2}{\mu^2} \left( 4\Sigma + \frac{q^2 Q^2}{\mu^2} \right)} \right], \quad (4.29)$$

valid for a specific radius  $r$  where  $\Sigma = r^2 - 3Mr + 2Q^2$ , valid for a specific radius  $r$ .

### 4.3.2 Zero angular momentum observers

To clarify the scenario in which circular orbits are possible, it is instructive to examine the behavior of zero angular momentum observers (ZAMOs). ZAMOs are observers characterized by their 4-velocity  $u$  which is a normalized linear combination of the two given Killing vectors in the spacetime geometry. These observers move in such a way that their motion is orthogonal to the  $\partial_\varphi$  direction, corresponding to the azimuthal coordinate, and they are future-pointing. and future-pointing, and it is the unit normal to the time coordinate hypersurfaces,

$$u = \Gamma(\partial_t + \zeta\partial_\varphi), \quad (4.30)$$

in other words it is tangent to a timelike spatially circular orbit.

A suitable orthonormal frame adapted to ZAMOs is given by

$$e_{\hat{t}} = \frac{1}{\sqrt{g_{00}}}\partial_t, \quad e_{\hat{r}} = \frac{1}{\sqrt{g_{11}}}\partial_r, \quad e_{\hat{\theta}} = \frac{1}{\sqrt{g_{22}}}\partial_\theta, \quad e_{\hat{\varphi}} = \frac{1}{\sqrt{g_{33}}}\partial_\varphi, \quad (4.31)$$

and the dual

$$\omega^{\hat{t}} = \sqrt{g_{00}}dt, \quad \omega^{\hat{r}} = \sqrt{g_{11}}dr, \quad \omega^{\hat{\theta}} = \sqrt{g_{22}}d\theta, \quad \omega^{\hat{\varphi}} = \sqrt{g_{33}}d\varphi. \quad (4.32)$$

The observer (4.30) can be parametrized equivalently either by the constant angular velocity  $\zeta$  with respect to infinity ( $d\varphi/dt$ ) or by the constant relative velocity  $\nu$  with respect ZAMOs,

$$u = \Gamma(\partial_t + \zeta\partial_\varphi) \equiv \gamma(e_{\hat{t}} + \nu e_{\hat{\varphi}}), \quad (4.33)$$

where  $\Gamma = -(-g_{00} - \zeta^2 g_{33})^{-1}$  and  $\gamma^2 = (1 - \nu^2)^{-1}$ . These quantities guarantee that  $u_\alpha u^\alpha = -1$ .

As we talk about  $\zeta$  being the constant angular velocity, we can define it with respect to  $\nu$ ,

$$\eta = \sqrt{-\frac{g_{00}}{g_{33}}}\nu.$$

It will be easier to continue from here using the explicitly equation of motion for a charged particle in RN spacetime,

$$u_\nu \nabla^\nu u_\alpha = \frac{q}{\mu} F_\alpha{}^\lambda u_\lambda, \quad (4.34)$$

the symmetry adapted frame has constant components, so the equation above becomes

$$e_{\hat{\nu}}\Gamma^{\hat{\nu}}_{\hat{\beta}\hat{\alpha}}e^{\hat{\beta}} = \frac{q}{\mu}F_{\hat{\alpha}}^{\hat{\lambda}}e_{\hat{\lambda}} \Rightarrow \gamma(\nu^2 - \nu_g^2) + \frac{\nu_g}{\zeta_g} \frac{qQ}{\mu r^2} = 0, \quad (4.35)$$

where

$$\zeta_g = \pm \frac{\sqrt{Mr - Q^2}}{r^2}, \quad \nu_g = \sqrt{\frac{Mr - Q^2}{\Delta}}. \quad (4.36)$$

So, we can get the linear velocity  $\nu \equiv \pm\nu_{\pm}^{(q)}$  of a charged particle for a given value of  $qQ/\mu$ ,

$$\nu \equiv \nu_{\pm}^{(q)} = \nu_g \sqrt{1 - \frac{q^2 Q^2}{2\mu^2 \zeta_g^2 \nu_g} \pm \frac{|q|Q}{\mu \zeta_g \nu_g r^2} \sqrt{\frac{1}{\gamma_g^2} + \frac{q^2 Q^2 \nu_g^2}{4\mu^2 \zeta_g^2} r^4}}, \quad (4.37)$$

where

$$\gamma_g = \sqrt{\frac{\Delta}{r^2 - 3Mr + 2Q^2}}.$$

If we use  $q = 0$ , then  $\nu = \pm\nu_g$ , what will be the linear velocity of a neutral particle. From now on, we will introduce two dimensionless parameters,

$$\bar{q} = \frac{q}{\mu}, \quad \bar{q}_0 = \frac{\nu_g \zeta_g r^2}{Q} \equiv \frac{Mr - Q^2}{Q\sqrt{\Delta}}, \quad (4.38)$$

using it in equation (4.35), we have

$$\frac{\bar{q}}{\bar{q}_0} = \gamma \left( 1 - \frac{\nu^2}{\nu_g^2} \right), \quad (4.39)$$

and rewritten the equation (4.37) we have

$$\nu_{\pm}^{(q)} = \nu_g \sqrt{\Lambda \pm \sqrt{\Lambda^2 - 1 + (\bar{q}/\bar{q}_0)^2}}, \quad (4.40)$$

where

$$\Lambda = 1 - \frac{\nu_g^2}{2} \left( \frac{\bar{q}}{\bar{q}_0} \right)^2. \quad (4.41)$$

Now we can investigate two situations:  $q < 0$  and  $q > 0$ . The first one can be understood by looking the equation (4.39), which implies  $q < 0 \Rightarrow \nu^2 > \nu_g^2$  ( $\mu$  is a positive

parameter and we are considering  $r > r_+ \Rightarrow \bar{q}_0 > 0$ ). It will give us a minimum radius  $r_\gamma$  such that  $\nu^2 = \nu_g^2$  when  $r = r_\gamma$ , defined due to equations (4.40) and (4.36),

$$\Lambda = 1 - \frac{1}{2} \left( \frac{\bar{q}}{\bar{q}_0} \right)^2 \quad (\text{or } \nu_g^2 = 1) \Rightarrow r_\gamma^2 - 3Mr_\gamma + 2Q^2 = 0, \quad (4.42)$$

so,  $\nu$  can exist only for  $r \geq r_\gamma^+$ , where

$$r_\gamma^+ = \frac{1}{2} \left( 3M + \sqrt{9M^2 - 8Q^2} \right). \quad (4.43)$$

On the other hand, we also have  $q > 0$ . In this case, solutions can exist for  $r_+ < r < r_\gamma^+$ . It will depend on the considered range of values of  $q$ . Looking at equation (4.39), to have  $q > 0$ , then  $\nu_g^2 > \nu^2 \geq 0$ , the maximal limit gives  $r = r_\gamma^+$  while the minimal give us a new condition

$$\Lambda \pm \sqrt{\Lambda^2 - 1 + (\bar{q}/\bar{q}_0)^2} \geq 0, \quad (4.44)$$

to ensure the existence of such velocities, we also have

$$\Lambda^2 - 1 + (\bar{q}/\bar{q}_0)^2 \geq 0. \quad (4.45)$$

The condition described in (4.45) give us a minimum radius

$$\Lambda^2 = 1 - \left( \frac{\bar{q}}{\bar{q}_0} \right)^2 \Rightarrow r_l^2 - 3Mr_l + 2Q^2 + \frac{1}{4}\bar{q}^2Q^2 = 0, \quad (4.46)$$

so,  $\nu$  can exist only for  $r \geq r_l$ , where

$$r_l = \frac{1}{2} \left( 3M + \sqrt{9M^2 - 8Q^2 - \bar{q}^2Q^2} \right). \quad (4.47)$$

To guarantee that  $r_l$  is real, we will have a new bound in  $\bar{q}$ , such that,  $9M^2 - 8Q^2 - \bar{q}^2Q^2 \geq 0$ , i.e., we have a maximal charge  $\bar{q}_l$ ,

$$\bar{q}_l = \frac{\sqrt{9M^2 - 8Q^2}}{Q}, \quad (4.48)$$

where  $\bar{q} \leq \bar{q}_l$ .

Looking the equation (4.39), if we make  $\bar{q} = \bar{q}_0$  it will imply in  $\nu^2 = 0$  and automatically in  $\gamma = 1$ .

This condition is the same described in (4.44) and (4.45) if  $(\bar{q}/\bar{q}_0)^2 - 1 = 0$  then we can satisfy both at the same time as long as  $\Lambda = 0$ . It will give us

$$\Lambda = 0 \Rightarrow 2r_s^2 - 5Mr_s + 3Q^2 = 0, \quad (4.49)$$

where

$$r_s = \frac{Q^2}{\bar{q}^2 Q^2 - M^2} \left[ M(\bar{q}^2 - 1) + \sqrt{\bar{q}^2(\bar{q}^2 - 1)(M^2 - Q^2)} \right], \quad (4.50)$$

and as  $r_s > r_+ > 0$  it implies in  $\bar{q}^2 Q^2 - M^2 > 0 \Rightarrow \bar{q} > M/Q$ .

So, we have

$$\frac{\bar{q}}{\bar{q}_0} > 1, \text{ then } r > r_s, \quad (4.51)$$

while

$$\frac{\bar{q}}{\bar{q}_0} < 1, \text{ then } r_+ < r < r_s. \quad (4.52)$$

However, the condition  $\nu = 0$  implies in other condition about  $\Lambda$ . Looking at equation (4.40) and making it equal 0 when  $\bar{q}/\bar{q}_0 = 1$  and  $r = r_s$ , we have

$$\Lambda(r_s) \pm \sqrt{\Lambda^2(r_s)} = 0, \quad (4.53)$$

for  $\nu_-^{(q)}$  it's trivially 0, but we also have  $2\Lambda(r_s) = 0$  and it's interesting to note that it is the same condition that we obtain when we want to satisfy the condition described in (4.44) using  $r = r_l$ .

In other words:  $\Lambda(r_s) = \Lambda(r_l) = 0$ , what give us a new condition

$$\Lambda(r_{s/l}) = 0 \Rightarrow 3M^2 - 2Q^2 + \bar{q}_s Q^2 + M\sqrt{9M^2 - 8Q^2 - \bar{q}_s^2} = 0, \quad (4.54)$$

where

$$\bar{q}_s = \frac{1}{\sqrt{2}Q} \sqrt{5M^2 - 4Q^2 + M\sqrt{25M^2 - 24Q^2}}. \quad (4.55)$$

The behavior of charged test particles depends strongly on their location with respect these special radii described before,  $r_+$ ,  $r_l$ ,  $r_\gamma^+$  and  $r_s$ .

As we already known, the particle's 4-momentum is given by  $P = mU - qQ$ . The conserved quantities associated with the temporal and azimuthal Killing vectors  $\xi = \partial_t$  and  $\eta = \partial_\varphi$  are, respectively,

$$P \cdot \xi = -\frac{\bar{q}Q}{r} - \gamma \frac{\sqrt{\Delta}}{r} = -\frac{E}{\mu} \quad (4.56)$$

$$P \cdot \eta = \frac{r}{M} \gamma \nu = \frac{h}{M\mu}. \quad (4.57)$$

Now we can separate it in 3 cases:

1.  $\bar{q} < 0$ :

The solution are geodesic velocities  $\nu = \pm\nu_+^{(q)}$  in the range  $r \geq r_\gamma^+$ . Orbits with  $r = r_\gamma^+$  are lightlike.

2.  $\bar{q} = 0$ :

The solution are geodesic velocities  $\nu = \pm\nu_g$  in the range  $r \geq r_\gamma^+$ .

3.  $\bar{q} > 0$ :

It will give us completely different subcases.

(a)  $\bar{q} < M/Q$ :

The solution are two different branches for both signs of the linear velocity:  $\nu = \pm\nu_+^{(q)}$  in the range  $r_l \leq r \leq r_\gamma^+$  and  $\nu = \pm\nu_-^{(q)}$  in the range  $r \geq r_l$ . Both branches join at  $r = r_l$ , where  $\nu_+^{(q)} = \nu_-^{(q)} = \nu_g \sqrt{\Lambda}$ .

(b)  $M/Q < \bar{q} < \bar{q}_s$ :

Since  $\bar{q}_s < \bar{q}_0$ , so we are looking at the case where  $\bar{q}/\bar{q}_0 < 1$  what implies that both solutions  $\nu_\pm^{(q)}$  can exist. The solution are two different branches for both signs of the linear velocity:  $\nu = \pm\nu_+^{(q)}$  in the range  $r_l \leq r \leq r_\gamma^+$  and  $\nu = \pm\nu_-^{(q)}$  in the range  $r_l \leq r \leq r_s$ . Both branches join at  $r = r_l$ .

(c)  $\bar{q}_s < \bar{q} < \bar{q}_l$ :

Different for the previous case, here  $\bar{q}/\bar{q}_0 > 1$  what implies that solution  $\nu_-^{(q)}$  for linear velocity is not allowed. The linear velocity will be  $\nu = \pm\nu_+^{(q)}$  in the range  $r_s < r < r_\gamma^+$ .

(d)  $\bar{q} > \bar{q}_l$ :

It will be like the previous case, but now  $r_l$  doesn't exist. The linear velocity will be  $\nu = \pm\nu_+^{(q)}$  in the range  $r_s < r < r_\gamma^+$ . It's important to note that when  $\epsilon \rightarrow +\infty \therefore r_s \rightarrow r_+$ .

We want the closest orbits possible what give us cases 3 (d).

# 5 Analytical Solutions

To construct a GF or just be able to calculate some of those interesting quantities (amplification factor, QNMs, etc), we need to solve the equation (3.3) at least in some convenient regime, and it is exactly what we are going to do: solve it in different regions of  $r$  (and some limits of frequencies) and matching those solutions.

## 5.1 Sub-extremal solutions: $Q < M$

The first step will be to redefine the radial variable  $r$ , define new constants,

$$x = \frac{r - r_+}{r_+}, \quad \tau = \frac{r_+ - r_-}{r_+}, \quad \hat{\omega} = \omega r_+, \quad \varpi = \hat{\omega} - qQ, \quad (5.1)$$

and with that change, the equation (3.3) can be written as

$$x^2(x + \tau)^2 R'' + (2x + \tau)x(x + \tau)R' + \left[ (x + 1)^2 (\varpi + \hat{\omega}x)^2 - x(x + \tau)\lambda_\ell \right] R = 0 \quad (5.2)$$

### 5.1.1 Solution valid for quasinormal modes

To construct that kind of solution will be useful to define one more constant  $k = 2\hat{\omega} - qQ$ , and using this constant in equation (5.2), we have

$$x^2(x + \tau)^2 R'' + (2x + \tau)x(x + \tau)R' + \left[ \frac{K^2}{r_+^2} - x(x + \tau)\lambda_\ell \right] R = 0, \quad (5.3)$$

where  $K/r_+ = \hat{\omega}x^2 + kx + \varpi$ .

#### 5.1.1.1 Near event horizon solution ( $x \ll 1$ )

The radial equation can be approximated by

$$x^2(x + \tau)^2 R'' + (2x + \tau)x(x + \tau)R' + \left[ (kx + \varpi)^2 - x(x + \tau)\lambda_\ell \right] R = 0. \quad (5.4)$$

and we have just two linearly independent solutions that satisfy a purely ingoing and/or outgoing boundary condition:

$$\begin{aligned}
R &= c_1 x^{-i\frac{\varpi}{\tau}} (x + \tau)^{-ik+i\frac{\varpi}{\tau}} {}_2F_1\left(\frac{1}{2} - ik + i\delta, \frac{1}{2} - ik - i\delta, 1 - 2i\frac{\varpi}{\tau}, -\frac{x}{\tau}\right) \\
&+ c_2 x^{+i\frac{\varpi}{\tau}} (x + \tau)^{+ik-i\frac{\varpi}{\tau}} {}_2F_1\left(\frac{1}{2} + ik + i\delta, \frac{1}{2} + ik - i\delta, 1 + 2i\frac{\varpi}{\tau}, -\frac{x}{\tau}\right)
\end{aligned} \quad (5.5)$$

where  $\delta^2 = k^2 - (\ell + 1/2)^2$ .

What gives to us:

$$R^{(\text{in})} = c_1^{(\text{in})} x^{-i\frac{\varpi}{\tau}} (x + \tau)^{-ik+i\frac{\varpi}{\tau}} {}_2F_1\left(\frac{1}{2} - ik + i\delta, \frac{1}{2} - ik - i\delta, 1 - 2i\frac{\varpi}{\tau}, -\frac{x}{\tau}\right), \quad (5.6)$$

and

$$\begin{aligned}
R^{(\text{up})} &= c_1^{(\text{up})} x^{-i\frac{\varpi}{\tau}} (x + \tau)^{-ik+i\frac{\varpi}{\tau}} {}_2F_1\left(\frac{1}{2} - ik + i\delta, \frac{1}{2} - ik - i\delta, 1 - 2i\frac{\varpi}{\tau}, -\frac{x}{\tau}\right) \\
&+ c_2^{(\text{up})} x^{+i\frac{\varpi}{\tau}} (x + \tau)^{+ik-i\frac{\varpi}{\tau}} {}_2F_1\left(\frac{1}{2} + ik + i\delta, \frac{1}{2} + ik - i\delta, 1 + 2i\frac{\varpi}{\tau}, -\frac{x}{\tau}\right)
\end{aligned} \quad (5.7)$$

where

$$c_1^{(\text{in})} = \frac{1}{r_+} \tau^{ik-i\frac{\varpi}{\tau}}, \quad c_2^{(\text{in})} = 0 \quad (5.8)$$

#### 5.1.1.2 Far region ( $x \gg \max(\tau, \varpi)$ ):

using a double limit  $\tau \rightarrow 0$ ,  $\varpi \rightarrow 0$  the equation (5.2) can be approximated by

$$x^2 R'' + 2xR' + [(\hat{\omega}x + k)^2 - \lambda_\ell] R = 0, \quad (5.9)$$

and the most general solution that satisfies a purely ingoing and/or outgoing boundary condition will be:

$$R = c_3 e^{-i\hat{\omega}x} x^{-\frac{1}{2}+i\delta} {}_1F_1\left(\frac{1}{2} + ik + i\delta, 1 + 2i\delta, 2i\hat{\omega}x\right) + c_4 (\delta \rightarrow -\delta) \quad (5.10)$$

What gives to us

$$R^{(\text{in/up})} = c_3^{(\text{in/up})} e^{-i\hat{\omega}x} x^{-\frac{1}{2}+i\delta} {}_1F_1\left(\frac{1}{2} + ik + i\delta, 1 + 2i\delta, 2i\hat{\omega}x\right) + c_4^{(\text{in/up})} (\delta \rightarrow -\delta) \quad (5.11)$$

### 5.1.1.3 Matching ( $\max(\tau, \varpi) \ll x \ll 1$ ):

using matched asymptotic expansions (MAE) we are able to define  $c_3$  and  $c_4$  ( $c_1$  and  $c_2$ ) for in(up)-modes solutions, while  $c_1$  and  $c_2$  ( $c_3$  and  $c_4$ ).

We have

$$c_3^{(\text{in})} = \frac{\tau^{\frac{1}{2}-ik-i\delta}\Gamma(2i\delta)\Gamma\left(1-\frac{2i\varpi}{\tau}\right)}{\Gamma\left(\frac{1}{2}-ik+i\delta\right)\Gamma\left(\frac{1}{2}+ik+i\delta-\frac{2i\varpi}{\tau}\right)}, \quad c_4^{(\text{in})} = c_3^{(\text{in})}(\delta \rightarrow -\delta). \quad (5.12)$$

And finally,

$$A_{\ell\omega}^{(\text{in})} = \frac{\Gamma(1+2i\delta)}{\Gamma\left(\frac{1}{2}-ik+i\delta\right)}(-2i\hat{\omega})^{-\frac{1}{2}-ik-i\delta}c_3^{(\text{in})} + \frac{\Gamma(1-2i\delta)}{\Gamma\left(\frac{1}{2}-ik-i\delta\right)}(-2i\hat{\omega})^{-\frac{1}{2}-ik+i\delta}c_4^{(\text{in})} \quad (5.13)$$

$$A_{\ell\omega}^{(\text{out})} = \frac{\Gamma(1+2i\delta)}{\Gamma\left(\frac{1}{2}+ik+i\delta\right)}(2i\hat{\omega})^{-\frac{1}{2}+ik-i\delta}c_3^{(\text{in})} + \frac{\Gamma(1-2i\delta)}{\Gamma\left(\frac{1}{2}+ik-i\delta\right)}(2i\hat{\omega})^{-\frac{1}{2}+ik+i\delta}c_4^{(\text{in})} \quad (5.14)$$

## 5.1.2 Solution valid for branch point

Now we will return to the equation (5.2).

### 5.1.2.1 Near event horizon ( $\hat{\omega}x \ll \varpi$ ):

the radial equation can be approximated by

$$x^2(x+\tau)^2R'' + (2x+\tau)x(x+\tau)R' + [(\varpi x + \varpi)^2 - x(x+\tau)\lambda_\ell]R = 0, \quad (5.15)$$

which is an equation identical to the equation 5.4 doing  $k \rightarrow \varpi$ . Giving us the same solution with the previous transformation.

$$R = \bar{c}_1 x^{-i\frac{\varpi}{\tau}}(x+\tau)^{-i\varpi+i\frac{\varpi}{\tau}} {}_2F_1\left(\frac{1}{2}-i\varpi+i\delta, \frac{1}{2}-i\varpi-i\delta, 1-2i\frac{\varpi}{\tau}, -\frac{x}{\tau}\right) + \bar{c}_2 x^{+i\frac{\varpi}{\tau}}(x+\tau)^{+i\varpi-i\frac{\varpi}{\tau}} {}_2F_1\left(\frac{1}{2}+i\varpi+i\delta, \frac{1}{2}+i\varpi-i\delta, 1+2i\frac{\varpi}{\tau}, -\frac{x}{\tau}\right), \quad (5.16)$$

where

$$R^{(\text{in})} = \bar{c}_1^{(\text{in})} x^{-i\frac{\varpi}{\tau}}(x+\tau)^{-i\varpi+i\frac{\varpi}{\tau}} {}_2F_1\left(\frac{1}{2}-i\varpi+i\delta, \frac{1}{2}-i\varpi-i\delta, 1-2i\frac{\varpi}{\tau}, -\frac{x}{\tau}\right) \quad (5.17)$$

and

$$\begin{aligned}
R^{(\text{up})} &= \bar{c}_1^{(\text{up})} x^{-i\frac{\varpi}{\tau}} (x + \tau)^{-i\varpi + i\frac{\varpi}{\tau}} {}_2F_1\left(\frac{1}{2} - i\varpi + i\delta, \frac{1}{2} - i\varpi - i\delta, 1 - 2i\frac{\varpi}{\tau}, -\frac{x}{\tau}\right) \\
&+ \bar{c}_2^{(\text{up})} x^{+i\frac{\varpi}{\tau}} (x + \tau)^{+i\varpi - i\frac{\varpi}{\tau}} {}_2F_1\left(\frac{1}{2} + i\varpi + i\delta, \frac{1}{2} + i\varpi - i\delta, 1 + 2i\frac{\varpi}{\tau}, -\frac{x}{\tau}\right)
\end{aligned} \tag{5.18}$$

where

$$\bar{c}_1^{(\text{in})} = \frac{1}{r_+} \tau^{i\varpi - i\frac{\varpi}{\tau}}, \quad \bar{c}_2^{(\text{in})} = 0 \tag{5.19}$$

### 5.1.2.2 Far region ( $x \gg \max(\tau, \varpi)$ ):

the equation (5.2) using the limit  $\tau \rightarrow 0$  but not  $\varpi \rightarrow 0$  we have

$$x^2 R'' + 2xR' + [(\hat{\omega}x + \varpi)^2 - \lambda_\ell] R = 0, \tag{5.20}$$

which, again, is an equation identical to the equation (5.9) doing  $k \rightarrow \varpi$ . Giving us the same solutions,

$$R = \bar{c}_3 e^{-i\hat{\omega}x} x^{-\frac{1}{2} + i\delta} {}_1F_1\left(\frac{1}{2} + i\varpi + i\delta, 1 + 2i\delta, 2i\hat{\omega}x\right) + \bar{c}_4 (\delta \rightarrow -\delta), \tag{5.21}$$

What gives to us

$$R^{(\text{in/up})} = \bar{c}_3^{(\text{in/up})} e^{-i\hat{\omega}x} x^{-\frac{1}{2} + i\delta} {}_1F_1\left(\frac{1}{2} + i\varpi + i\delta, 1 + 2i\delta, 2i\hat{\omega}x\right) + \bar{c}_4^{(\text{in/up})} (\delta \rightarrow -\delta) \tag{5.22}$$

where  $\bar{c}_n$  with  $n = 1, \dots, 4$  are constants and  $\bar{\delta}^2 = \varpi^2 - (\ell + 1/2)^2$ .

### 5.1.2.3 Matching ( $\varpi \ll x \ll \varpi/\hat{\omega}$ ):

using MAE we are able to define  $\bar{c}_3$  and  $\bar{c}_4$  ( $\bar{c}_1$  and  $\bar{c}_2$ ) for in(up)-modes solutions, while  $\bar{c}_1$  and  $\bar{c}_2$  ( $\bar{c}_3$  and  $\bar{c}_4$ ) will be founded according to the defined tortoise, coordinate  $r_*$  showed in equation (3.4).

We have

$$\bar{c}_3^{(\text{in})} = \frac{\tau^{\frac{1}{2} - i\varpi - i\delta} \Gamma(2i\delta) \Gamma\left(1 - \frac{2i\varpi}{\tau}\right)}{\Gamma\left(\frac{1}{2} - i\varpi + i\delta\right) \Gamma\left(\frac{1}{2} + i\varpi + i\delta - \frac{2i\varpi}{\tau}\right)}, \quad \bar{c}_4^{(\text{in})} = \bar{c}_3^{(\text{in})} (\delta \rightarrow -\delta). \tag{5.23}$$

And finally,

$$\begin{aligned}
\bar{A}_{\ell\omega}^{(\text{in})} &= \frac{\Gamma(1+2i\delta)}{\Gamma\left(\frac{1}{2}-i\varpi+i\delta\right)} (-2i\hat{\omega})^{-\frac{1}{2}-i\varpi-i\delta} c_3^{(\text{in})} + \frac{\Gamma(1-2i\delta)}{\Gamma\left(\frac{1}{2}-i\varpi-i\delta\right)} (-2i\hat{\omega})^{-\frac{1}{2}-i\varpi+i\delta} c_4^{(\text{in})} \\
\bar{A}_{\ell\omega}^{(\text{out})} &= \frac{\Gamma(1+2i\delta)}{\Gamma\left(\frac{1}{2}+i\varpi+i\delta\right)} (2i\hat{\omega})^{-\frac{1}{2}+i\varpi-i\delta} c_3^{(\text{in})} + \frac{\Gamma(1-2i\delta)}{\Gamma\left(\frac{1}{2}+i\varpi-i\delta\right)} (2i\hat{\omega})^{-\frac{1}{2}+i\varpi+i\delta} c_4^{(\text{in})}
\end{aligned} \tag{5.25}$$

## 5.2 Extremal solutions: $Q = M$

The first step will be to redefine the radial variable  $r$  and define a new constant:

$$x = \frac{r-M}{M}, \quad \alpha = 1 - \frac{\omega}{q}, \quad \beta = qM, \tag{5.26}$$

and with that change, the equation (3.3) can be written as

$$x^4 R'' + 2x^3 R' + \left[ \beta^2 (1+x)^2 (x(-1+\alpha) + \alpha)^2 - \lambda_\ell x^2 \right] R = 0, \tag{5.27}$$

### 5.2.1 Solution valid for superradiant bound frequencies

In this region we have  $\omega \sim \omega_{SR}$ , which for an extremal RN BH means,  $\omega \sim q$ . So, using our new constant  $\alpha$ , we are considering  $|\alpha| \leq 1$ .

#### 5.2.1.1 Near event horizon solution ( $x \ll 1/|\beta|$ ):

the radial equation can be approximated by

$$z^2 R'' + \left( \alpha^2 \beta^2 z^2 - 2\alpha\beta^2 z + (\beta^2 - \lambda_\ell) \right) R = 0, \tag{5.28}$$

where  $z = 1/x$ .

We have just two linearly independent solutions that satisfy a purely ingoing and/or outgoing boundary condition:

$$\begin{aligned}
R &= d_1 e^{-i\alpha\beta z} z^{\frac{1}{2}-i\delta} {}_1F_1\left(\frac{1}{2}-i\beta-i\delta, 1-2i\delta, 2i\alpha\beta z\right) \\
&+ d_2 e^{-i\alpha\beta z} z^{\frac{1}{2}+i\delta} {}_1F_1\left(\frac{1}{2}-i\beta+i\delta, 1+2i\delta, 2i\alpha\beta z\right).
\end{aligned} \tag{5.29}$$

What give to us

$$d_1^{(\text{in})} = \frac{(-2i\alpha\beta)^{-i\beta-i\delta+\frac{1}{2}} (-i\alpha\beta)^{2i\delta} \Gamma\left(\frac{1}{2}-i\beta-i\delta\right) \Gamma\left(\frac{1}{2}+i\beta\pm i\delta\right)}{\Gamma(1-2i\delta) \left[ (-i\alpha\beta)^{2i\delta} \Gamma\left(\frac{1}{2}\pm i\beta\pm i\delta\right) - (i\alpha\beta)^{2i\delta} \Gamma\left(\frac{1}{2}\pm i\beta\mp i\delta\right) \right]}, \quad d_2^{(\text{in})} = d_1^{(\text{in})} (\delta \rightarrow -\delta) \tag{5.30}$$

where:  $\Gamma(a \pm b \mp c) = \Gamma(a + b - c) \Gamma(a - b + c)$ .

### 5.2.1.2 Far region ( $x \gg |\alpha\beta|$ ):

the radial equation can be approximated by

$$x^2 R'' + 2xR' + (\beta^2 x^2 + 2\beta^2 x + (\beta^2 - \lambda_\ell)) R = 0, \quad (5.31)$$

and again we have

$$\begin{aligned} R^{(\text{in/up})} &= d_3^{(\text{in/up})} e^{-i\beta x} x^{-\frac{1}{2}+i\delta} {}_1F_1\left(\frac{1}{2} + i\beta + i\delta, 1 + 2i\delta, 2i\beta x\right) \\ &+ d_4^{(\text{in/up})} e^{-i\beta x} x^{-\frac{1}{2}-i\delta} {}_1F_1\left(\frac{1}{2} + i\beta - i\delta, 1 - 2i\delta, 2i\beta x\right), \end{aligned} \quad (5.32)$$

where  $\delta = \beta^2 - (\ell + 1/2)^2$ .

### 5.2.1.3 Matching ( $|\alpha\beta| \ll x \ll |\beta|^{-1}$ ):

as explained in the previously section, we will use MAE to define  $d_3$  and  $d_4$  ( $d_1$  and  $d_2$ ) for in(up)-modes solutions.

In this case, it will be a trivial relation:

$$d_3 = d_1, \quad d_4 = d_2. \quad (5.33)$$

And finally,

$$A_{\ell\omega}^{(\text{in})} = d_4^{(\text{in})} (-2i\beta)^{-\frac{1}{2}-i\beta+i\delta} \frac{\Gamma(1-2i\delta)}{\Gamma\left(\frac{1}{2}-i\beta-i\delta\right)} + d_3^{(\text{in})} (-2i\beta)^{-\frac{1}{2}-i\beta-i\delta} \frac{\Gamma(1+2i\delta)}{\Gamma\left(\frac{1}{2}-i\beta+i\delta\right)} \quad (5.34)$$

$$A_{\ell\omega}^{(\text{out})} = d_4^{(\text{in})} (2i\beta)^{-\frac{1}{2}+i\beta+i\delta} \frac{\Gamma(1-2i\delta)}{\Gamma\left(\frac{1}{2}+i\beta-i\delta\right)} + d_3^{(\text{in})} (2i\beta)^{-\frac{1}{2}+i\beta-i\delta} \frac{\Gamma(1+2i\delta)}{\Gamma\left(\frac{1}{2}+i\beta+i\delta\right)} \quad (5.35)$$

## 5.3 Quasinormal frequencies spectrum

As explained before, the QNMs are the roots of the Wronskian. This quantity was defined in equation (3.9). So, we need to make

$$A_{\ell\omega_{\ell n}}^{(\text{in})} = 0, \quad (5.36)$$

where  $\omega_{\ell n}$  are the QN-frequencies.

Using the equation (5.13), we have

$$\frac{\Gamma(1+2i\delta)}{\Gamma\left(\frac{1}{2}-ik+i\delta\right)}(-2i\hat{\omega})^{-\frac{1}{2}-ik-i\delta}c_3^{(\text{in})} + \frac{\Gamma(1-2i\delta)}{\Gamma\left(\frac{1}{2}-ik-i\delta\right)}(-2i\hat{\omega})^{-\frac{1}{2}-ik+i\delta}c_4^{(\text{in})} = 0 \quad (5.37)$$

and using also  $c_{3,4}^{(\text{in})}$  defined in (5.12),

$$\frac{\Gamma(1+2i\delta)\Gamma(2i\delta)(-2i\hat{\omega}\tau)^{-i\delta}}{\Gamma\left(\frac{1}{2}-ik+i\delta\right)^2\Gamma\left(\frac{1}{2}+ik+i\delta-\frac{2i\varpi}{\tau}\right)} + \frac{\Gamma(1-2i\delta)\Gamma(-2i\delta)(-2i\hat{\omega}\tau)^{i\delta}}{\Gamma\left(\frac{1}{2}-ik-i\delta\right)^2\Gamma\left(\frac{1}{2}+ik-i\delta-\frac{2i\varpi}{\tau}\right)} = 0. \quad (5.38)$$

This equation is valid in the limit  $\tau \ll 0$ ,  $\omega \simeq qQ/r_+(\varpi \ll 0)$ , where this equation can be solved analytically. We need to write it in the following form:

$$\Gamma\left(\frac{1}{2}+ik-i\delta-\frac{2i\varpi}{\tau}\right)^{-1} = \mathcal{D} \times (-2i\hat{\omega}\tau)^{-2i\delta}, \quad (5.39)$$

where

$$\mathcal{D} = \frac{\Gamma(2i\delta)^2\Gamma\left(\frac{1}{2}-ik-i\delta\right)^2}{\Gamma(-2i\delta)^2\Gamma\left(\frac{1}{2}-ik+i\delta\right)^2\Gamma\left(\frac{1}{2}+ik+i\delta-\frac{2i\varpi}{\tau}\right)}. \quad (5.40)$$

In the limit  $\omega \rightarrow qQ/r_+$ , being  $\omega$  almost purely real, we can see that  $\delta^2$  is also almost purely real. If  $\delta \gtrsim 1$ . Then one has  $(-i)^{-2i\delta} = e^{-\pi\delta} \ll 1$ . Therefore we find  $\epsilon \equiv (-2i\hat{\omega}\tau)^{-2i\delta} \ll 1$ .

A consistent solution of the condition (5.39) can be obtained if  $1/\Gamma\left(\frac{1}{2}+ik-i\delta-\frac{2i\varpi}{\tau}\right) = O(\epsilon)$ . Suppose

$$\frac{1}{2}+ik-i\delta-\frac{2i\varpi}{\tau} = -n + \eta\epsilon + O(\epsilon^2) \quad (5.41)$$

where  $n \geq 0$  is a non-negative integer and  $\eta$  is a constant to be defined. Using the previous equation into the gamma function, we get

$$\Gamma\left(\frac{1}{2}+ik-i\delta-\frac{2i\varpi}{\tau}\right) \simeq \Gamma(-n + \eta\epsilon), \quad (5.42)$$

using the following property of the gamma function:

$$\Gamma(-n + \eta\epsilon) = (\eta\epsilon - n)^{-1}\Gamma(-n + 1 + \eta\epsilon),$$

expanding in  $\epsilon$  we have

$$(\eta\epsilon - n)^{-1} = (-n)^{-1} + n^{-2}\eta\epsilon + O(\epsilon^2)$$

finally we get

$$\Gamma\left(\frac{1}{2} + ik - i\delta - \frac{2i\varpi}{\tau}\right) \simeq (-n)^{-1}\Gamma(-n + 1 + \eta\epsilon). \quad (5.43)$$

This new gamma function can be written as

$$\Gamma(-n + 1 + \eta\epsilon) = (-1)^{n-1} \frac{\Gamma(-1 - \eta\epsilon)}{\Gamma(n - \eta\epsilon)} \eta\epsilon(\eta\epsilon + 1)\Gamma(\eta\epsilon)$$

and expanding this coefficient,

$$\frac{\Gamma(-1 - \eta\epsilon)}{\Gamma(n - \eta\epsilon)} \eta\epsilon(\eta\epsilon + 1) = \Gamma(n)^{-1} + O(\epsilon^2),$$

using this relation in equation (5.43),

$$\Gamma\left(\frac{1}{2} + ik - i\delta - \frac{2i\varpi}{\tau}\right) \simeq \frac{(-1)^n}{n!} \Gamma(\eta\epsilon) + O(\epsilon),$$

and finally we have

$$\Gamma\left(\frac{1}{2} + ik - i\delta - \frac{2i\varpi}{\tau}\right)^{-1} \simeq (-1)^n n! \eta\epsilon + O(\epsilon^2) \quad (5.44)$$

using  $1/\Gamma(z) = z + O(z^2)$ . And now using the equation (5.44) into (5.39) we have

$$\eta = \frac{\mathcal{D}}{(-1)^n n!}. \quad (5.45)$$

Using the definitions  $\hat{\omega} = \omega r_+$ ,  $\varpi = \hat{\omega} - qQ$  and  $k = 2\hat{\omega} - qQ$  into the equation (5.41), will give us the QNM spectrum

$$\omega_{\ell n} = \frac{qQ}{r_+} - 2\pi i T_{\text{BH}} \left[ \left( \frac{1}{2} + n - \eta\epsilon \right) - i(\delta - qQ) \right], \quad (5.46)$$

where  $T_{\text{BH}} = (r_+ - r_-)/4\pi r_+^2$ .

## 5.4 Totally reflected frequencies spectrum

To have a TRM we need to make  $A_{\ell\bar{\omega}_{\ell n}}^{(\text{in})} \rightarrow \infty$ . Looking to the expression (5.13) with  $c_{3,4}^{(\text{in})}$  defined in (5.12), we can get

$$F(\omega)\Gamma\left(1 - \frac{2i\varpi}{\tau}\right)\tau^{\frac{1}{2}-ik} \quad (5.47)$$

where  $F(\omega)$  is the left side of equation (5.38) but, as  $\omega \neq \omega_{\ell n}$  it will not be zero. To make this equation diverge our best option is to make

$$1 - \frac{2i\varpi}{\tau} = -n, \quad (5.48)$$

where  $n \in \mathbb{Z}$ .

Using the definitions  $\hat{\omega} = \omega r_+$ ,  $\varpi = \hat{\omega} - qQ$ , we will have the TRM spectrum

$$\bar{\omega}_n = \frac{qQ}{r_+} - 2\pi iT_{\text{BH}}(1+n). \quad (5.49)$$

where  $T_{\text{BH}} = (r_+ - r_-)/4\pi r_+^2$ .



# 6 Numerical Solutions

To guarantee that our results are reliable, we needed to use numerical methods to solve the radial KG equation (3.3) for in and up-modes.

## 6.1 Sub-extremal solutions: $Q < M$

As explained before, the equation(3.3) has three singular points, where two of them regular ones. It gives us the possibility to construct an exact solution around these regular singular points using a Fröbenius series. Using it we can guarantee purely ingoing and/or outgoing solutions in the event horizon. Satisfying the condition of ingoing or outgoing waves at infinity will be difficult and we will resort to numerical methods using Mathematica, it will be clear later.

### 6.1.1 IN-modes solutions

We need to use a Möbius transformation and change the radial coordinate to  $z = (r - r_-)/(r_+ - r_-)$ , and it will map the singularities at

$$(r_-, r_+, +\infty) \rightarrow (0, 1, +\infty),$$

and now use  $R(r)$  as

$$R(z) \propto z^\eta (z - 1)^\xi e^{\zeta(r_+ - r_-)z} y(z), \quad (6.1)$$

to guarantee the shape of the confluent Heun equation and purely ingoing solution at the event horizon, these constants  $\eta$ ,  $\xi$  and  $\zeta$  will be

$$\eta = ir_- \frac{\omega r_- - qQ}{r_+ - r_-}, \quad \xi = -ir_+ \frac{\omega r_+ - qQ}{r_+ - r_-}, \quad \zeta = i\omega. \quad (6.2)$$

and then the radial KG equation (3.3) becomes

$$y''(z) + \left( \alpha + \frac{\beta}{z-1} + \frac{\gamma}{z} \right) y'(z) + \frac{\sigma z + \nu}{z(z-1)} y(z) = 0, \quad (6.3)$$

where

$$\alpha = 2\zeta(r_+ - r_-), \quad (6.4)$$

$$\beta = 1 + 2\xi, \quad (6.5)$$

$$\gamma = 1 + 2\eta, \quad (6.6)$$

$$\sigma = 2(r_+ - r_-) \left[ \zeta(1 + \eta + \xi) - (qQ - 2\omega)\omega - (r_+ + r_- - 2)\zeta^2 \right] \quad (6.7)$$

$$\begin{aligned} \nu = & q^2 Q^2 + \xi + \eta + (\xi + \eta)^2 - 2qQ(2 + r_-)\omega + 4\omega^2 - 2Q^2\omega^2 \quad (6.8) \\ & + 4r_- \omega^2 - \lambda - [r_- + 2r_- \xi - 4(1 + \eta + \xi) + r_+(3 + 4\eta + 2\xi)] \zeta \\ & + [2r_+ r_- + (r_+ - 2)^2 - 2Q^2 - r_-^2] \zeta^2. \end{aligned}$$

As we saw before, we have three singular points:  $z = 0, 1, \infty$ . Being the two first ones regular ones and, being so, we can construct Fröbenius solutions around that points. Since the exponents at  $z = 0$  are 0 and  $1 - \gamma$ , let  $\text{HeunC}(-\nu, \sigma, \gamma, \beta, \alpha, z)$  be the regular solution at  $z = 0$ , we choose the following normalization

$$\text{HeunC}(-\nu, \sigma, \gamma, \beta, \alpha, 0) = 1, \quad (6.9)$$

and around  $z = 0$  we have two local solutions

$$y_{01}(z) = \text{HeunC}(-\nu, \sigma, \gamma, \beta, \alpha, z) \quad (6.10)$$

$$y_{02}(z) = z^{1-\gamma} \text{HeunC}[(\alpha - \beta)(1 - \gamma) - \nu, \alpha(1 - \gamma) + \sigma, 2 - \gamma, \beta, \alpha, z]. \quad (6.11)$$

Analogously, around  $z = 1$ , we have

$$y_{11}(z) = \text{HeunC}(-\sigma - \nu, -\sigma, \beta, \gamma, -\alpha, 1 - z) \quad (6.12)$$

$$\begin{aligned} y_{12}(z) = & (1 - z)^{1-\beta} \quad (6.13) \\ & \times \text{HeunC}[(\beta - 1)(\alpha + \gamma) - \sigma - \nu, \alpha(\beta - 1) - \sigma, 2 - \beta, \gamma, -\alpha, 1 - z]. \end{aligned}$$

The solution  $y_{11}$  is the one that satisfies the boundary condition to have in-modes, (3.7), and will be what we choose. So, our exact solution, near the event horizon is defined by

$$R_{\text{num}}^{(\text{in})}(z) = c_H z^\eta (z - 1)^\xi e^{\zeta(r_+ - r_-)z} \text{HeunC}(-\sigma - \nu, -\sigma, \beta, \gamma, -\alpha, 1 - z) \quad (6.14)$$

where all constants are defined previously and  $c_H$  is a constant defined using the tortoise coordinate. And reinforcing: this solution is valid for any charge  $Q$  and  $q$ , any frequency  $\omega$ , and any integer value of  $\ell$ , but only near the event horizon.

To use this solution will also be fundamental as a tool to obtain numerically QNMs. We can use a method presented by Fiziev in [Fiziev 2007].

We have this local solution (6.14) around  $z = 1 \therefore r = r_+$ . To have a QNM we should guarantee purely out-going waves at  $z \rightarrow \infty \therefore r \rightarrow \infty$  and it is a problem for two reasons in this case: the first one is because  $z \rightarrow \infty$  is an irregular singular point, as we already knew, what makes it impossible for us to construct a regular solution using a Frobenius series just like we did previously using HeunC; the second reason is the presence of a BC for  $z \in (1, \infty)$  in a HeunC function, Motygin showed it very well in [Motygin 2018], it can be seen in Figure 1.

However, any solution of an ODE can be represented by a linear combination of local solutions. And more than that, we can write a local solution around a singular point  $X$  as a linear combination of solutions around  $Y$ , where in this case  $X, Y = 0, 1, \infty$ . Something like  $R_{x1,2} = \Gamma_{X1,2}^{Y1} R_{Y1} + \Gamma_{X1,2}^{Y2} R_{Y2}$ , the problem is: this ‘‘connection coefficient’’ is unknown for confluent Heun functions. But for our case we only need to guarantee that the coefficient multiplying the solution at  $z \rightarrow 0$  for purely out-going waves be 0, and Fiziev realized this technique in section 4.2 for a static BH. We need to impose:

$$\lim_{|z| \rightarrow \infty} \left| R_{\text{num}}^{(\text{in})} \left[ |z| e^{-i\left(\frac{\pi}{2} + \arg(-\omega)\right)} \right] \right| = 0, \quad (6.15)$$

then we will use:

$$\left| R_{\text{num}}^{(\text{in})} \left[ z_{\infty} e^{-i\left(\frac{\pi}{2} + \arg(-\omega)\right)} \right] \right| = 0, \quad (6.16)$$

where  $z_{\infty} \gg 1$ . Fiziev also showed that for  $z_{\infty} \geq 20$  the QNMs have essentially the same value, with a slightly difference appearing in the 8th decimal place comparing  $z_{\infty} = 20$  and 100, it was showed in Table 3 of Fiziev’s work.

#### 6.1.1.1 Comparing solutions:

Having defined analytical solutions considering frequencies near the superradiant-bound limit (subsection 5.1.1) and also the case with small-frequencies (subsection 5.1.2) and a general numerical solution defined in equation (6.14) valid near the event horizon, we can compare both of them. We will show it for different charges of the BH, different  $\ell$ -modes and these two frequency-regimes.

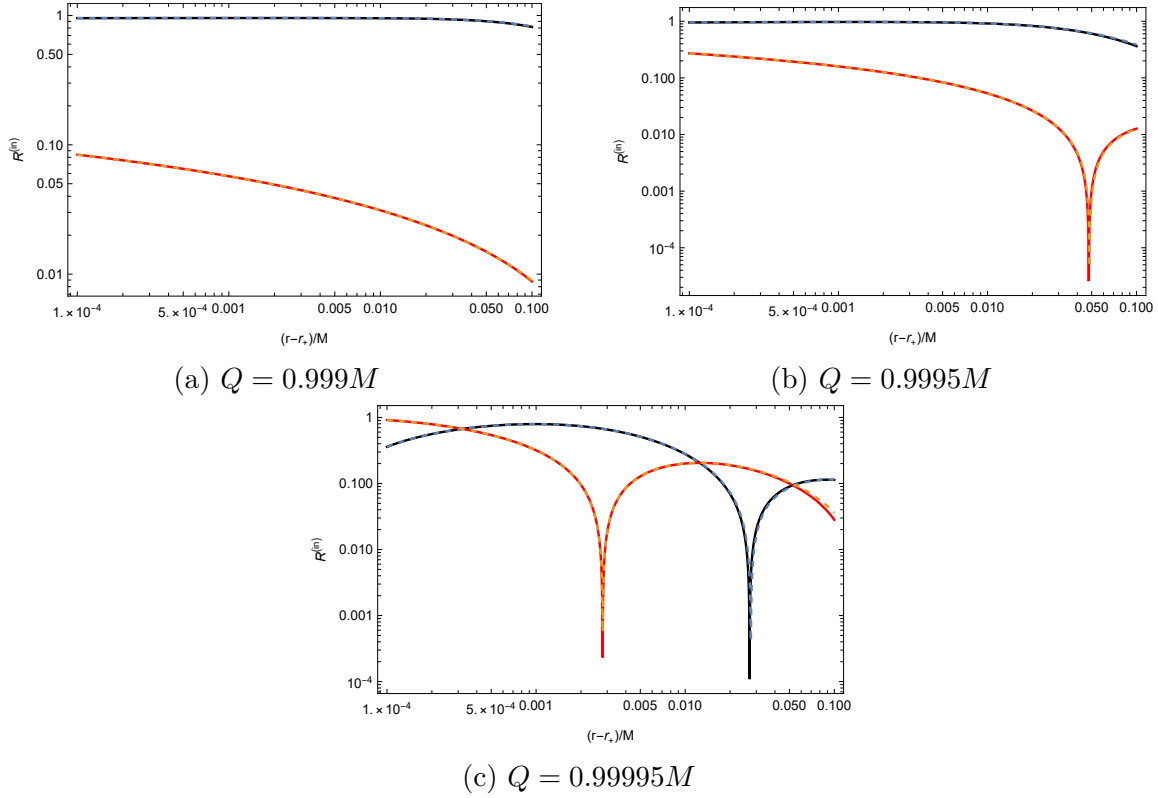


Figure 2 – LogLog-plots of real and imaginary parts of  $R^{(\text{in})}$  being black and red ones numerical, blue and orange analytical solutions. We are using  $qM = 1$ ,  $\ell = 0$  and  $\omega M = \omega_{\text{SR}}M + 0.001$ .

### 6.1.2 UP-modes solutions

To obtain our UP-solutions we'll use the purely out-going at infinity boundary condition (3.8), using a suitable large radius denoted by  $r_{\text{inf}}$ , denoting

$$f_{\ell\omega}^{(\text{up})} \sim r_*^{-iqQ} e^{i\omega r_*}, \quad (6.17)$$

and then the initial conditions for  $f_{\ell\omega}^{(\text{up})}$  and  $f'_{\ell\omega}^{(\text{up})}$  evaluated at  $r_{\text{inf}}$ :

$$f_{\ell\omega}^{(\text{up})}(r_{\text{inf}}) = r_*(r_{\text{inf}})^{-iqQ} e^{i\omega r_*(r_{\text{inf}})}, \quad (6.18)$$

$$f'_{\ell\omega}^{(\text{up})}(r_{\text{inf}}) = \frac{d}{dr} \left( r_*^{-iqQ} e^{i\omega r_*} \right)_{r=r_{\text{inf}}}, \quad (6.19)$$

these initial conditions become more accurate as  $r_{\text{inf}}$  increase.

We compute the initial conditions (6.18) and (6.19) in Mathematica for  $r_{\text{inf}} = 10^3 M$ . Having computed the boundary conditions, we then used Mathematica's `NDSolve` function to generate our UP-modes for our given  $Q$ ,  $q$ ,  $\omega$  and  $\ell$ . We set `WorkingPrecision` to around 30, `AccuracyGoal` to around 24 and `PrecisionGoal` to around 12.

So, our solution will be:

$$R^{(\text{up})}(r) = \frac{1}{r} f_{\ell\omega}^{(\text{up})}(r). \quad (6.20)$$

Is important to remember: this solution is valid for any value of charge  $Q$  and  $q$ , any frequency  $\omega$  and any  $\ell$ , since we are obeying the range  $r \in [r_0, r_{\text{inf}}]$ . We have defined  $r_{\text{inf}}$  but will be more interesting to define  $r_0$  further and the reason will be explained.

### 6.1.2.1 Comparing solutions:

Having defined analytical solutions considering frequencies near the superradiant-bound limit (subsection 5.1.1) and also the case with small-frequencies (subsection 5.1.2) and a general numerical solution defined in equation (6.14) valid near the event horizon, we can compare both of them. We will show it for different charges of the BH, different  $\ell$ -modes and these two frequency-regimes.

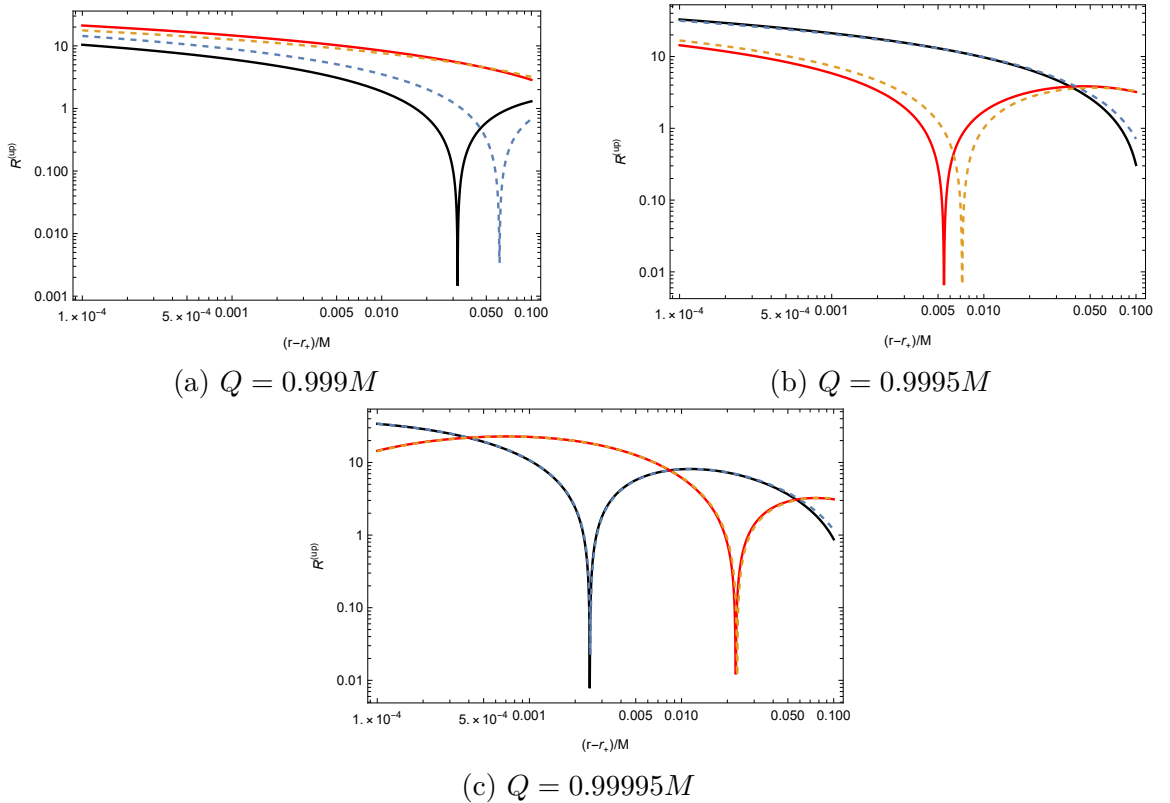


Figure 3 – LogLog-plots of real and imaginary parts of  $R^{(\text{up})}$  being black and red ones numerical, blue and orange analytical solutions. We are using  $qM = 1$ ,  $\ell = 0$  and  $\omega M = \omega_{\text{SR}} M + 0.001$ .

## 6.2 Extremal solutions: $Q = M$

As explained before in subsection 3.1.2, the equation (3.10) has two singular points both of them irregular. So, we cannot construct an exact solution around these points using a series like Fröbenius as we did for a sub-extremal BH around the event horizon. And the boundary conditions are defined in  $r = M$  and  $r \rightarrow +\infty$ , which are precisely the the singular points.

So, the way that we found was the same to treat UP-modes solutions in the sub-extremal case. Solving numerically using Mathematica.

### 6.2.1 IN-modes solutions

To obtain our IN-solutions we will use the purely in-going at the event horizon boundary condition (3.7), using a suitable close to  $M$  radius denoted by  $r_0$ . We have

$$f_{\ell\omega}^{(\text{in})} \sim e^{\frac{iM^2}{r-M}(\omega-q)}(r-M)^{-iM(2\omega-q)}, \quad (6.21)$$

and then the initial conditions for  $f_{\ell\omega}^{(\text{in})}$  and  $f'_{\ell\omega}^{(\text{in})}$  evaluated at  $r_0$ :

$$f_{\ell\omega}^{(\text{in})}(r_0) = e^{\frac{iM^2}{r_0-M}(\omega-q)}(r_0-M)^{-iM(2\omega-q)}, \quad (6.22)$$

$$f'_{\ell\omega}^{(\text{in})}(r_0) = \frac{d}{dr} \left( e^{\frac{iM^2}{r-M}(\omega-q)}(r-M)^{-iM(2\omega-q)} \right)_{r=r_0} \quad (6.23)$$

these initial conditions become more accurate as  $r_0$  is close to  $M$ .

We compute the initial conditions (6.22) and (6.23) in Mathematica for  $r_0 = (1 + 10^{-3})M$ . Having computed the boundary conditions, we then used Mathematica's `NDSolve` function to generate our IN-modes for our given  $q$ ,  $\omega$  and  $\ell$ . We set `WorkingPrecision` to around 30, `AccuracyGoal` to around 24 and `PrecisionGoal` to around 12.

So, our solution will be:

$$R^{(\text{in})}(r) = \frac{1}{r} f_{\ell\omega}^{(\text{in})}(r). \quad (6.24)$$

Is important to remember: this solution is valid for any value of charge  $q$ , any frequency  $\omega$  and any  $\ell$ , since we are obeying the range  $r \in [r_0, r_{\text{inf}}]$ .

### 6.2.2 UP-modes solutions

Will be exactly the same process shown in subsection 6.1.2, using the same  $r_{\text{inf}}$  and the same numerical precision. We will just need to use the boundary condition defined in (3.8).

# 7 Results

## 7.1 Spectroscopy analysis

### 7.1.1 Superradiance

The amplification factor  $Z_{\ell\omega}$  was described in the expression (3.16), and we can reproduce this quantity analytically for two different regimes of frequencies: when  $\omega \sim \omega_{\text{SR}}$  and also when  $\omega M \ll 1$  using  $A_{\ell\omega}^{(\text{in})}$  defined, respectively, in (5.13) and (5.24).

Numerically we can study a larger range of frequency and will be more convenient to redefine  $Z_{\ell\omega}$  using the wronskian,

$$Z_{\ell\omega} = - \left( 1 - \frac{qQ}{\omega r_+} \right) \frac{4\omega^2}{|\mathcal{W}_{\ell\omega}|^2}, \quad (7.1)$$

where this definition, just like the previous one, works to sub-extremal and extremal RN BH just being necessary to change the wronskian in these two cases. As we said before  $\omega \in \mathbb{R}$ .

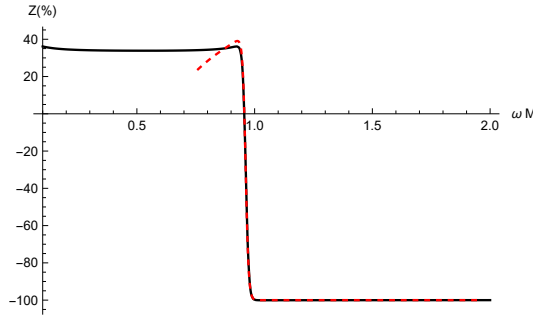


Figure 4 – Amplification factor  $Z_{0\omega}$  (in percentage form) as a function of the frequency with  $qQ = 0.999$ . The red dashed curve is the approximation in subsection 5.1.1.

The wronskian in this region near the superradiant-bound limit, defined for near-extremal BH (5.13) and also for extremal BH (5.34), lead to two distinct behaviors of  $Z_{\ell\omega}$  depending if  $\delta^2$  is positive or negative. Looking at the extremal case is more interesting, and will be the context where we will explore firstly. When  $\delta^2 < 0$ , we have that  $Z \rightarrow 0$  as  $\alpha \rightarrow 0 \therefore \omega \rightarrow \omega_{\text{SR}}$  and  $Z$  is continuous at  $\alpha = 0$ , it can be seen in figure 5b; in this case  $Z$  has a trivial behavior varying monotonically in  $\alpha$ . Otherwise, when  $\delta^2 \geq 0$  this implies that  $Z$  has a discontinuity at  $\alpha = 0$ , but more than that,  $Z$  presents an infinity number of oscillations as far as  $\alpha \rightarrow 0$  for negative and positive values of  $\alpha$ , it is completely analogous to what happens in Kerr spacetime and was described for the first time by Starobinsky in [Starobinsky 1974].

It is exemplified in figure 5a and also the emergence of this oscillations as far as  $Q \rightarrow M$  in 6.

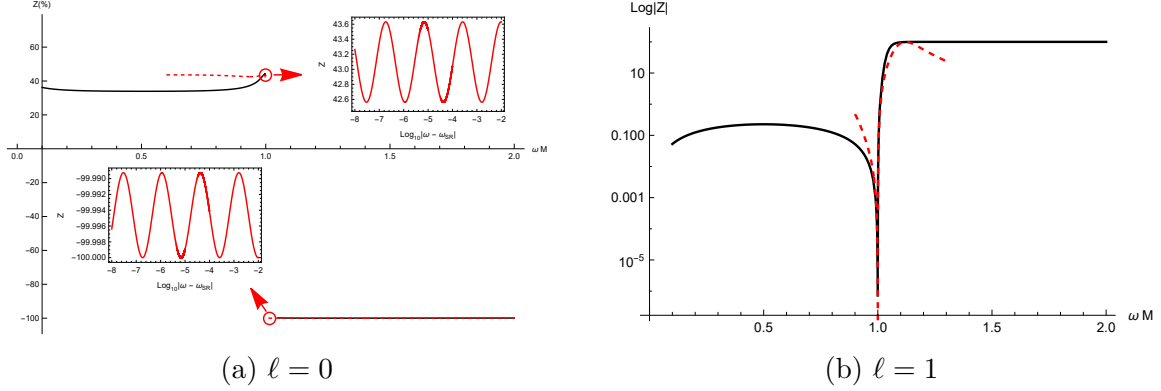


Figure 5 – Plots of  $Z_{\ell\omega}$  for  $Q = M$ ,  $qQ = 1$ . The black lines are numerical solutions while dashed red ones using  $A_{\ell\omega}^{(\text{in})}$  defined in (5.34). In the left we zoomed very close the superradiant-bound limit from left and from right to show the infinity oscillations, analytically it can also be seen in equation (7.2).

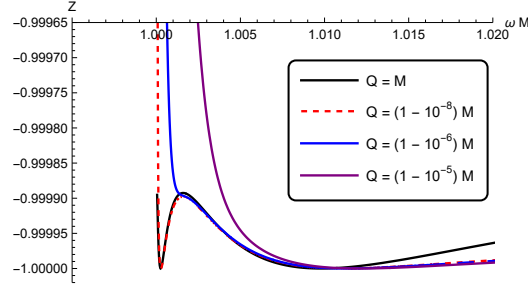


Figure 6 – Amplification factor  $Z_{0\omega}$  as a function of the frequency for different values of  $Q$  and  $qM = 10$ . For  $Q < M$  we are considering the  $A_{\ell\omega}^{(\text{in})}$  defined in (5.13) and when  $Q = M$  the  $A_{\ell\omega}^{(\text{in})}$  defined in (5.34).

In the case where  $\delta^2 > 0$ ,  $Z_{\ell\omega}$  in the extremal case can be rewrite as

$$Z_{\ell\omega} = e^{\pi\beta(\text{sign}(\alpha)-1)} \text{sh}^2(2\pi\delta) \text{sign}(\alpha) \times \left\{ \text{ch}^2\pi(\delta - \beta) e^{\pi\delta(\text{sign}(\alpha)-1)} + \text{ch}^2\pi(\beta + \delta) e^{-\pi\delta(\text{sign}(\alpha)-1)} + -2\text{ch}\pi(\beta - \delta) \text{ch}\pi(\beta + \delta) \cos \left[ \phi_0 - 2\delta \log \left( 4\beta^2 |\alpha| \right) \right] \right\}^{-1}, \quad (7.2)$$

where  $\phi_0 = \arg \left[ \Gamma(1 + 2i\delta)^4 \Gamma \left( \frac{1}{2} + i\beta - i\delta \right)^2 \Gamma \left( \frac{1}{2} - i\beta - i\delta \right)^2 \right]$ .

From now on we will consider  $\omega \in \mathbb{C}$ .

### 7.1.2 Modes in near-extremal Reissner-Nordström

We will study the QNMs described previously in section 5.3 by equation (5.46), and also the TRMs described in section 5.4 by equation (5.49).

### 7.1.2.1 Quasinormal modes properties:

we already knew from some references that for charged perturbations (scalar or spinorial ones) appears two families of QNMs as  $Q \rightarrow M$ : zero-damping modes (ZDMs) and damped-modes (DMs). The ZDMs are a kind of frequencies where the imaginary part vanishes as far as  $Q \rightarrow M$  at the same time that  $\omega \rightarrow \omega_{\text{SR}}$  and it was studied in [Richartz e Giugno 2014]. The DMs have the opposite behavior: the imaginary parts tends to a finite value and it was studied in [Cavalcante e Cunha 2021].

The ZDMs exist for every value of  $\ell$  and is exactly what we construct in the expression (5.46) calculated for the first time by Hod in [Hod 2010]. When  $Q \rightarrow M$ , consequently  $T_{\text{BH}} \rightarrow 0$  and the imaginary part vanishes for both cases. This causes and accumulation of ZDMs near the superradiant-bound frequency and can be seen in Figure 8.

The DMs on the other hand don't have an defined spectrum. For Kerr BH, is knew that this modes have  $|\Re\omega| > |\omega_{\text{SR}}|$  and a well defined condition of the existence. Is required that:  $\delta_K^2 + 1/4 < 0$  where  $\delta_K$  is an analogous quantity of our  $\delta$ , defined by  $\delta_K^2 = \lambda - m^2 + 1/4$ ; but  $\lambda$ , in Kerr spacetime is extremely more complicated, in which it depends of  $a$  (angular-velocity of the BH),  $\ell$  and  $\omega$ . In the eikonal limit ( $\ell \gg 1$ ) the existence condition becomes easier:  $\mu < \mu_c$  where  $\mu = m/(\ell + 1/2)$  and  $\mu_c \sim 0.74$ .

As we have seen, QNMs in RN spacetime do not depends on the azimuthal number  $m$  what could indicate that DMs would not exist in this spacetime. However, the quantity  $qQ$  appears for charged perturbations and works similarly with a significant difference,  $qQ$  is continuous while  $m$  is a discrete parameter.

Richartz in [Richartz 2016] have shown QNMs for extremal RN with  $\Im\omega \neq 0$  and  $|\Re\omega| > |\omega_{\text{SR}}|$  that survive when the BH becomes extremal, and more than that Richartz showed that for  $Q = 0.999M$  and  $Q = M$  the DMs will essentially have the same value with a difference starting in the 6th decimal place. Cavalcante & Carneiro in [Cavalcante e Cunha 2021] showed that exist a critical value of  $qQ$  and  $Q$  from which the fundamental QNM is a DM for  $\ell = 0$ . A very interesting plot in Figures 3 and 4 shows it. These critical values are:  $(qQ)_c \sim 0.216228$  and  $Q_c \sim 0.996917M$ . Figure 2 of Cavalcante & Carneiro shows the fundamental DM frequency that was showed by Richartz in Table VII for  $qQ = 0.1$  for instance, in this table Richartz shows 3 DMs.

Taking into account what Richartz showed about DMs for near-extremal RN BH we also have investigate DMs for higher values of  $qQ$  to compare with some interesting plots of Casals & Longo in [Casals e Micchi 2019], showing how similar RN and Kerr are when we are studying charged scalar perturbations (in RN spacetime) and scalar perturbations (in Kerr spacetime). We can see that DMs for Kerr have only 2 modes, Richartz showed it in Table I and Casals & Longo in a lot of Figures like Figure 7 and 9.

In Figure 7 we can see the accumulation of ZDMs (that will become a BC like in Casals & Longo's when  $Q = M$ ) and 3 DMs.

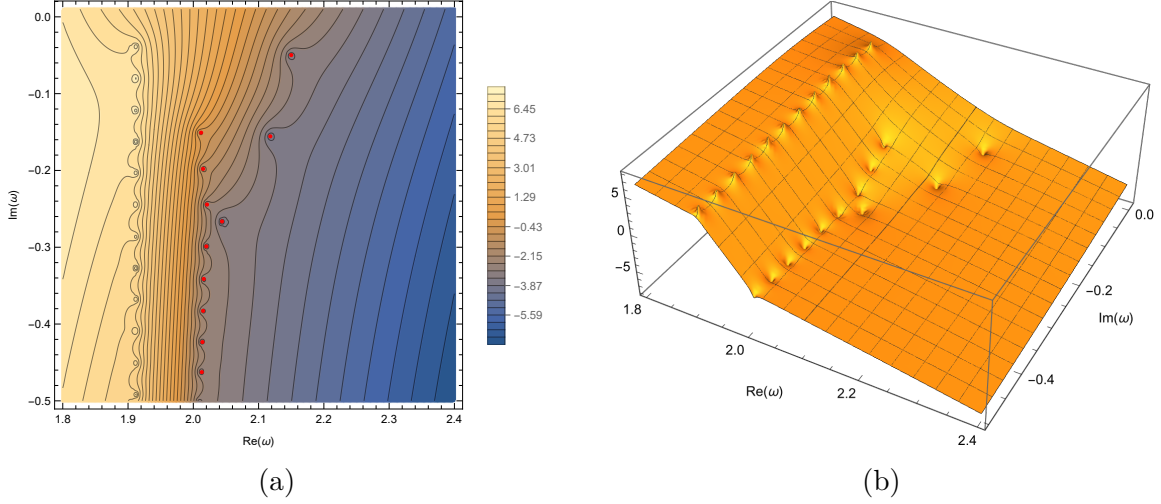


Figure 7 – Plots of (6.16) for  $Q = 0.999M$ ,  $q = 2/M$ ,  $\ell = 3$  and  $z_\infty = 20$ . We use a contour plot where the red dots are the QNMs on the left and a 3D plot on the right. For these values of charges,  $M\omega_{\text{SR}} \simeq 1.91249$  the QNMs with real part close to this value are ZDMs while the other 3 are DMs.

#### 7.1.2.2 Totally reflected modes properties:

Just like the QNMs, we already knew about this ones. We discuss about the TRMs in subsection 3.2.3 and in section 5.4 we constructed the spectrum described by expression (5.49). We will rewrite it here to be simpler to analyze:

$$\bar{\omega}_n = \frac{qQ}{r_+} - 2\pi iT_{\text{BH}}(1 + n). \quad (7.3)$$

In subsection 3.2.4 we talk about the emergence of a BC in the superradiant-bound frequency when the BH become extremal. And looking the spectrum of QNMs and TRMs it become more evident. The ZDM frequencies, discussed in the previous section, and the TRM frequencies have their imaginary parts being vanished as far as  $Q \rightarrow M$ , however, the effect in  $\mathcal{W}$  of this kind of frequencies is totally opposite as we can see in the expression (3.18), QNMs makes  $\mathcal{W} \rightarrow 0$  while TRMs makes  $\mathcal{W} \rightarrow \infty$ . In Figure 10 we can see these modes approaching each other until form the BC.

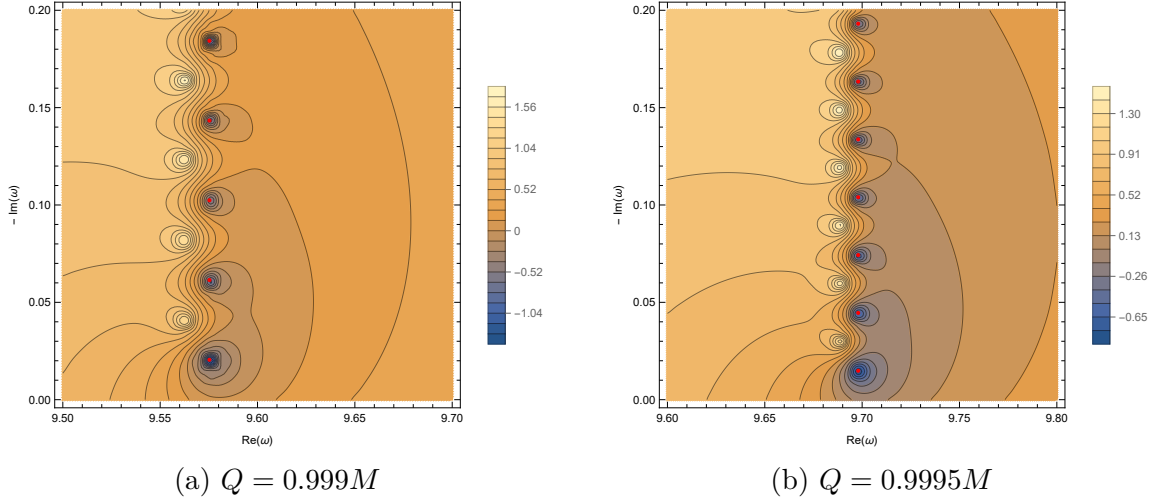


Figure 8 – Plots of  $\log_{10} |\mathcal{W}|$  for  $qM = 10$ . We are using  $A^{(\text{in})}_{\ell\omega}$  defined in (5.13). The mode is  $\ell = 2$ , and  $M\omega_{\text{SR}} \sim 9.56246$  and  $9.68866$ . The red dots are the QNMs.

### 7.1.3 Branch cuts

We investigate the presence of a BC in the complex-frequency plane, around the branch point at  $\omega = 0$  and at  $\omega = \omega_{\text{SR}}$  in extremal BH.

We calculated the wronskian for  $\omega = \omega_0 e^{i\phi}$  given some frequency  $\omega_0 \in \mathbb{C}$ , being in some cases  $\omega_0 \sim 0$  and  $\omega_0 \sim \omega_{\text{SR}}$ , varying the phase  $\phi \in [0, 2\pi]$ . The discontinuity is an indicator of a BC, and confirm it in Figures 9 for the superradiant BC and 11 for the BC at origin.

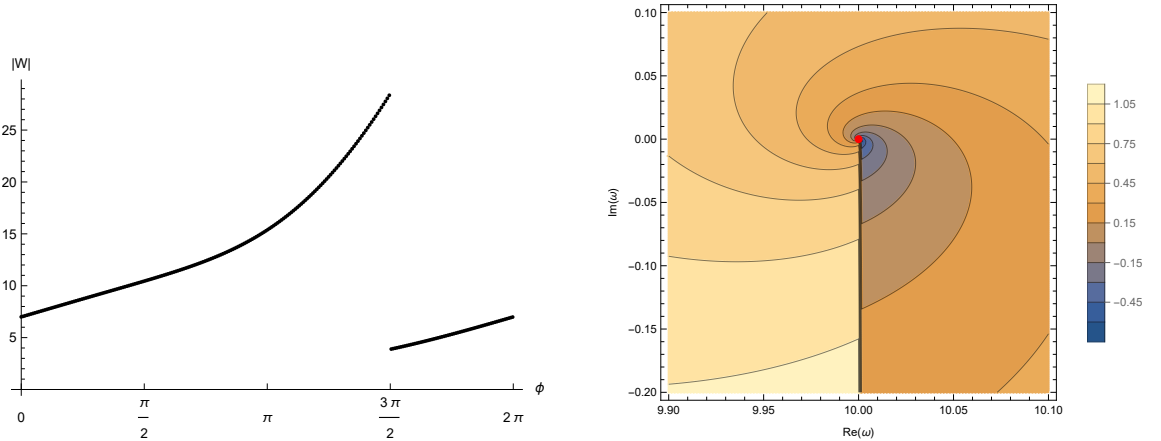


Figure 9 – Plots of  $|\mathcal{W}|$  as function of a phase  $\phi$  (left) and a contour plot of  $\log_{10} |\mathcal{W}|$  for  $Q = M$ ,  $qQ = 10$  and  $\ell = 2$ . We are using  $A^{(\text{in})}_{\ell\omega}$  defined in (5.34), the red dot at the center of the contour plot is  $\omega = \omega_{\text{SR}}$ .

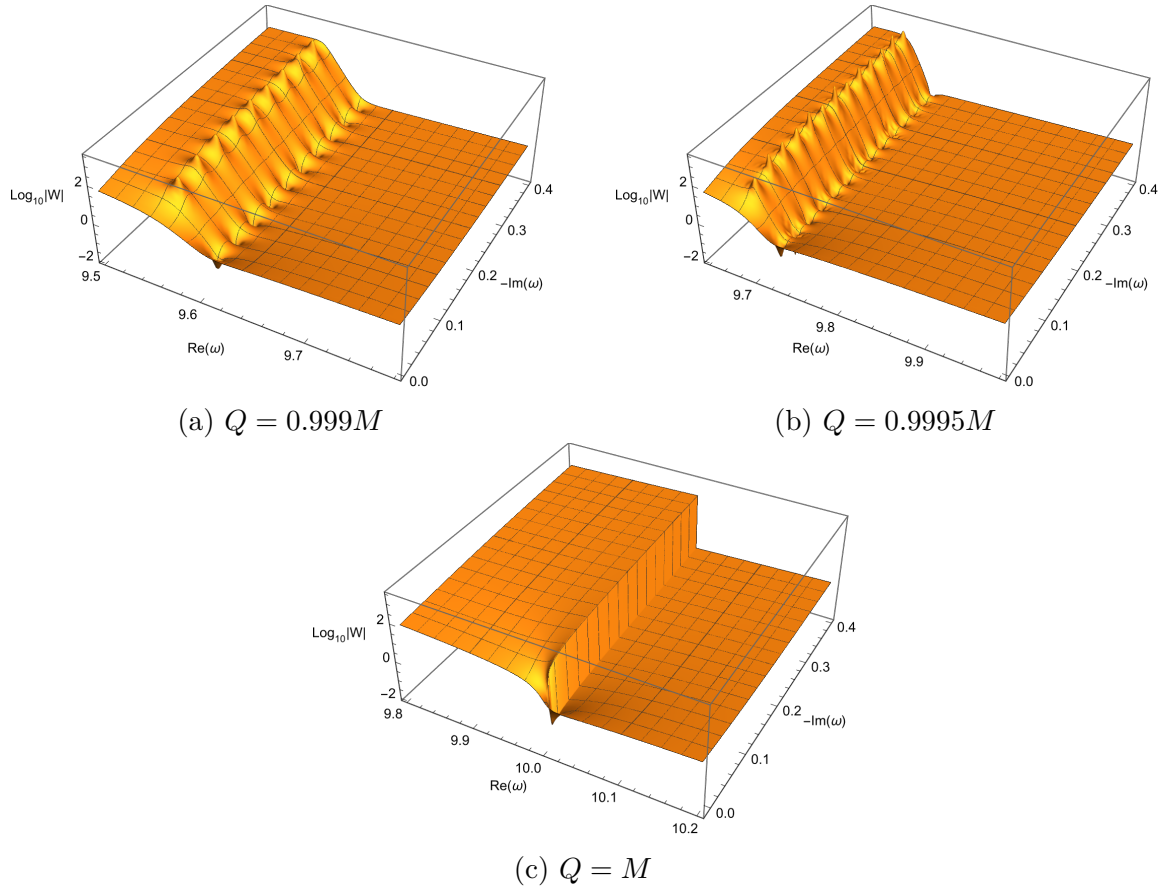


Figure 10 – Plots of  $\log_{10} |\mathcal{W}|$  for  $qM = 10$ . We are using  $A_{\ell\omega}^{(\text{in})}$  defined in (5.13) and (5.34) for  $Q < M$  and  $Q = M$ , respectively. The mode is  $\ell = 4$ , and  $M\omega_{\text{SR}} \simeq 9.56246$ ,  $9.68866$  and  $M\omega_{\text{SR}} = 10$  for the respective values of  $Q$ .

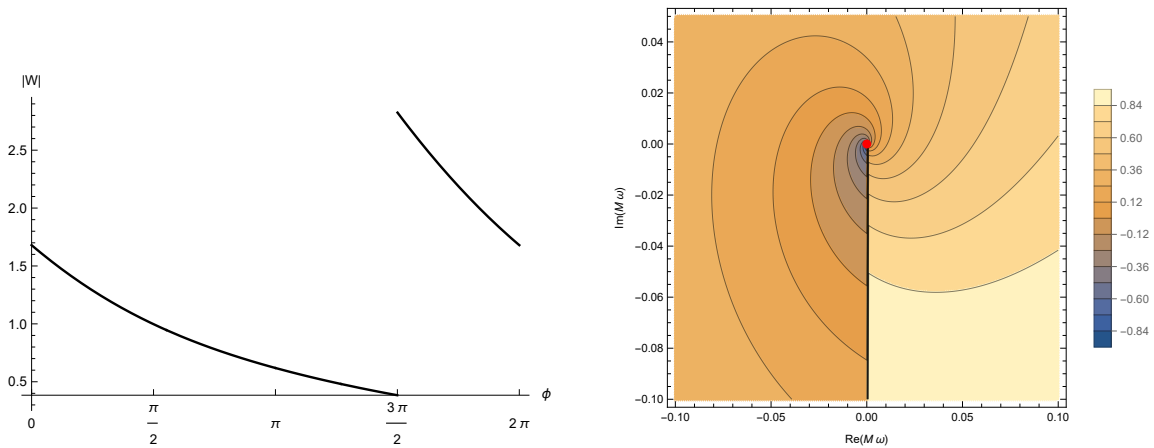


Figure 11 – Plots of  $|\mathcal{W}|$  as function of a phase  $\phi$  (left) and a contour plot of  $\log_{10} |\mathcal{W}|$  for  $Q = 0.999M$ ,  $qQ = 9.99$  and  $\ell = 2$ . We are using  $A_{\ell\omega}^{(\text{in})}$  defined in (5.24), the red dot at the center of the contour plot is  $\omega = 0$ .

## 7.2 Green Function analysis

Having defined all the important quantities now we are able to start to develop the GF for specific value of charges and radius.

We are interest in study orbits closest as possible to the event horizon (see the section 4.3) for a BH near-extremal.

As shown in subsection 4.3.2, we will use a charge-mass ratio  $q/\mu$  such that  $q/\mu > \bar{q}_l$  (case 3 (d)) what will give us a possible orbit for  $r_0 \sim r_+$ . We will take a look at the linear velocity, the energy and the angular momentum for a few different charges. The value of the charge-mass ratio will be  $q/\mu \equiv \bar{q} = 10$ , while  $\mu = 0.1M$ .

To define the BH charge we will use the smallest near-extremal value where  $R^{(\text{up})}$  has reasonable compatibility with numerical values while fix  $q/M = 1$ . We are guaranteeing that we have analytical field solution (described in subsection 5.1.1) compatible enough with the numerical solutions (described for IN solutions in subsection 6.1.1 and for UP solutions in subsection 6.1.2). We can see at figure Figure 3 that  $Q = 0.99995M$  is a good value to guarantee sufficient compatible solutions.

Along with these parameters, we were also able to define an orbit studying the linear velocity, energy and angular momentum of the particle, using  $r_0 = r_+ + 10^{-3}M$  what will give us a linear velocity  $\nu = 0.970326$ . The energy and angular momentum for the previous parameters will be:  $E = 9.90945M$  and  $h = 4.05705M$ .

So, reinforcing, we have:

$$\mu = 0.1M, \quad qM = 1, \quad \nu = 0.970326, \quad E = 9.90945M \quad \text{and} \quad h = 4.05705M \quad (7.4)$$

while  $Q = 0.99995M$  (therefore  $qQ = 0.99995$ ) and  $r_0 = r_+ + 10^{-3}M$ .

Now we are able to construct the Fourier-modes of the GF defined in (4.5). First we will compare the Wroskian, using (??) for different values of  $\ell$ , this will be important to understand in which range of  $\omega$  the solutions are compatible. As shown in Figure 12, they agree until  $\omega M = \omega_{\text{SR}}M \pm \epsilon M$ .

Investigating the numerator of the GF, that means,  $f_{\ell\omega}^{(\text{in})} f_{\ell\omega}^{(\text{up})}$ , Figure 13, we will see the same behavior as the wroskian  $\mathcal{W}_{\ell\omega}$ . And finally comparing the GF defined in (4.5) using numerics and analytical solutions, Figure 14, surprisingly we can see that both solutions keep being compatible even for values of  $\omega$  where  $\mathcal{W}_{\ell\omega}$  and  $f_{\ell\omega}^{(\text{in})} f_{\ell\omega}^{(\text{up})}$  are not.

Our goal is to integrate  $G_\ell$ , as shown in (4.3). We will integrate numerically the solution in a large range of  $\omega$  for  $\ell = 0$ , it together with our previous plots and argument will give us credibility to trust the results for different values of  $\ell$ . This will be discussed in more detail in the next section.

But the same for small-frequencies also need to be done, first looking the wronskian at Figure 15, then  $f_{\ell\omega}^{(\text{in})} f_{\ell\omega}^{(\text{up})}$  and GF can be shown in Figures 16 and 17, respectively.

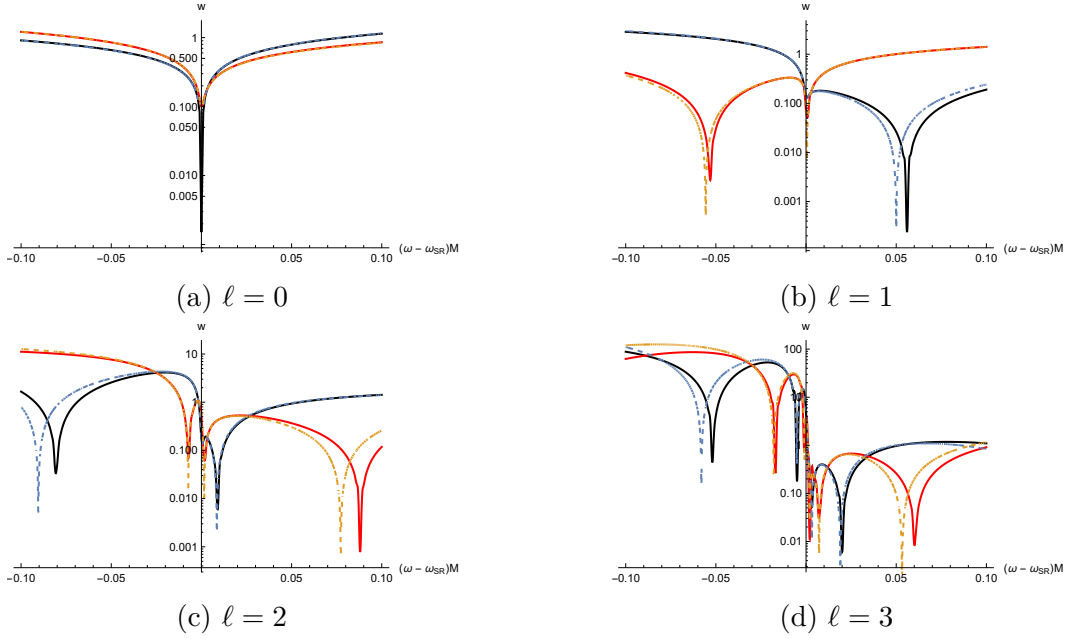


Figure 12 – Log-plots of the real and imaginary parts of  $\mathcal{W}_{\ell\omega}$  for different values of  $\ell$  defined using analytical and numerical solutions. Black and red are numerical solutions, while blue and orange the analytical ones, being black/blue real and red/orange imaginary parts around the SR-frequency.

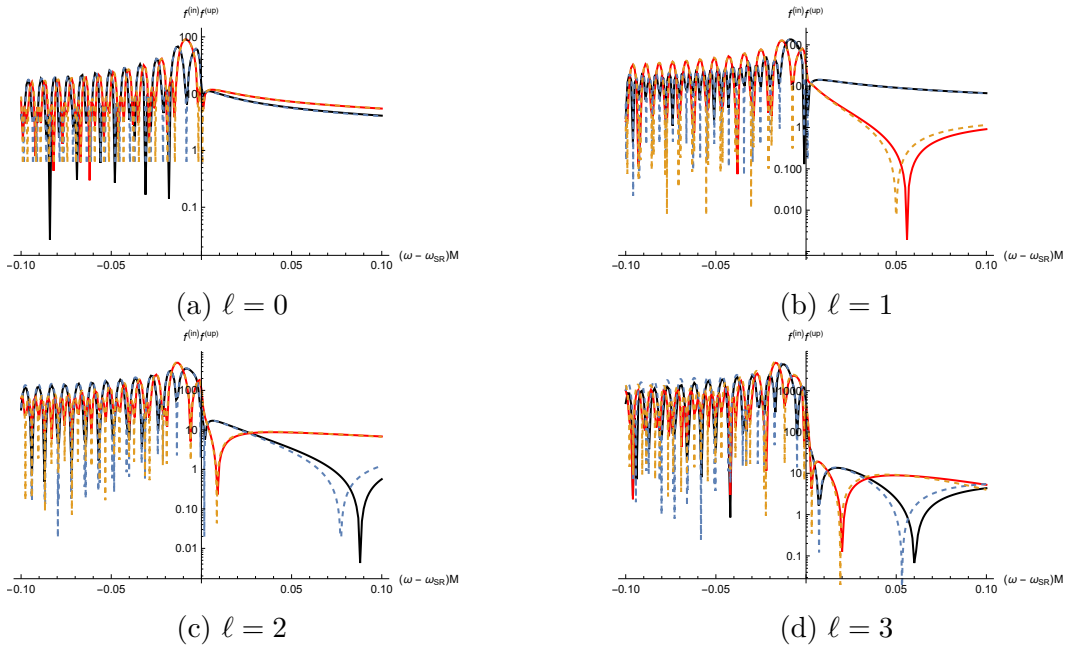


Figure 13 – Log-plots of the real and imaginary parts of  $f_{\ell\omega}^{(\text{in})} f_{\ell\omega}^{(\text{up})}$  for different values of  $\ell$  defined using analytical and numerical solutions. Black and red are numerical solutions, while blue and orange the analytical ones, being black/blue real and red/orange imaginary parts.

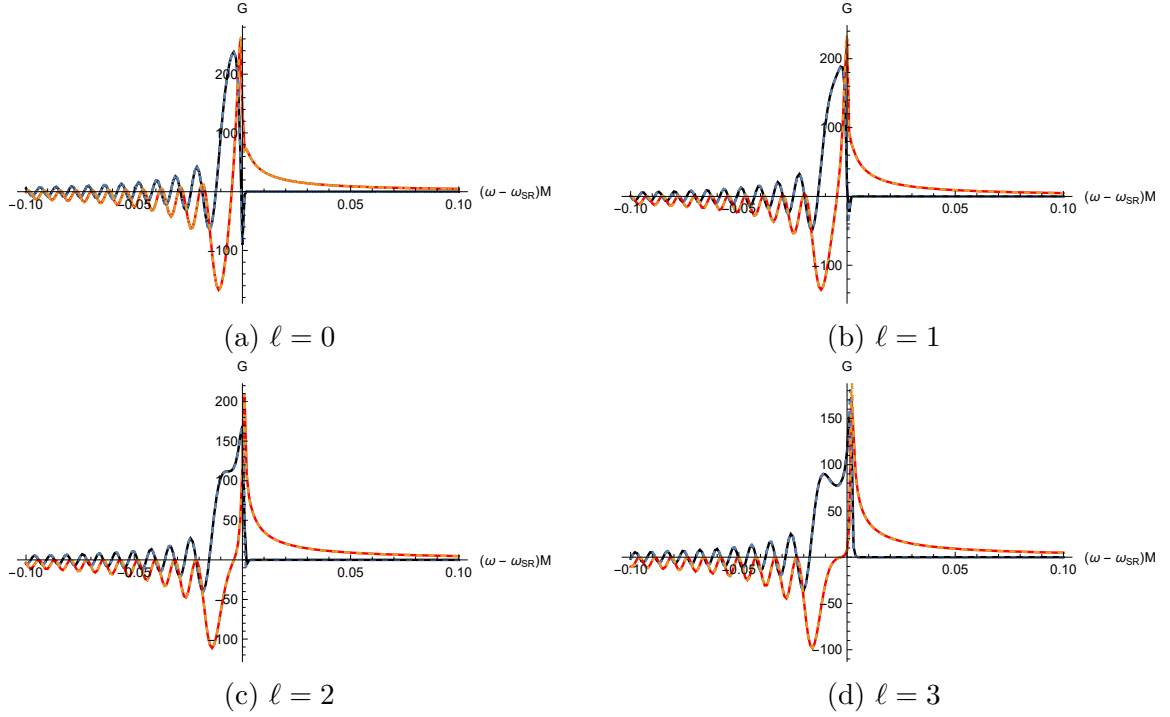


Figure 14 – Plots of the real and imaginary parts of  $G_\ell$  for different values of  $\ell$  defined using analytical and numerical solutions. Black and red are numerical solutions, while blue and orange the analytical ones, being black/blue real and red/orange imaginary parts.

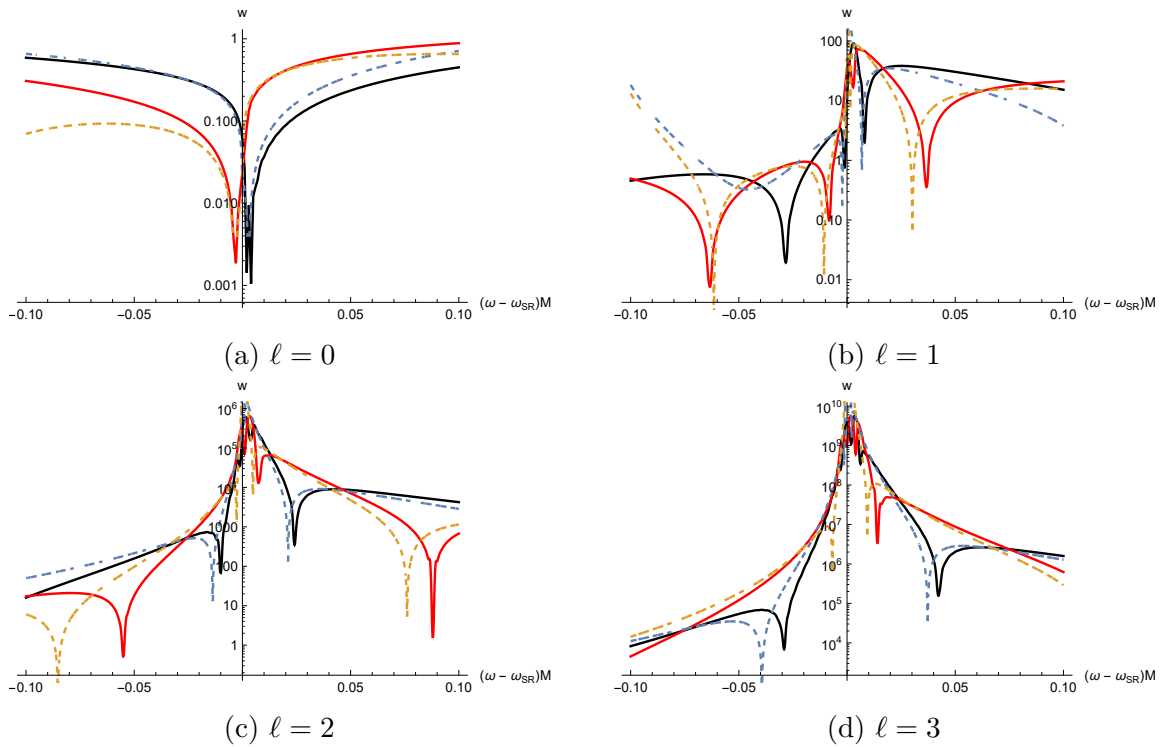


Figure 15 – Log-plots of the real and imaginary parts of  $\mathcal{W}_{\ell\omega}$  for different values of  $\ell$  defined using analytical and numerical solutions. Black and red are numerical solutions, while blue and orange the analytical ones, being black/blue real and red/orange imaginary parts for low-frequencies.

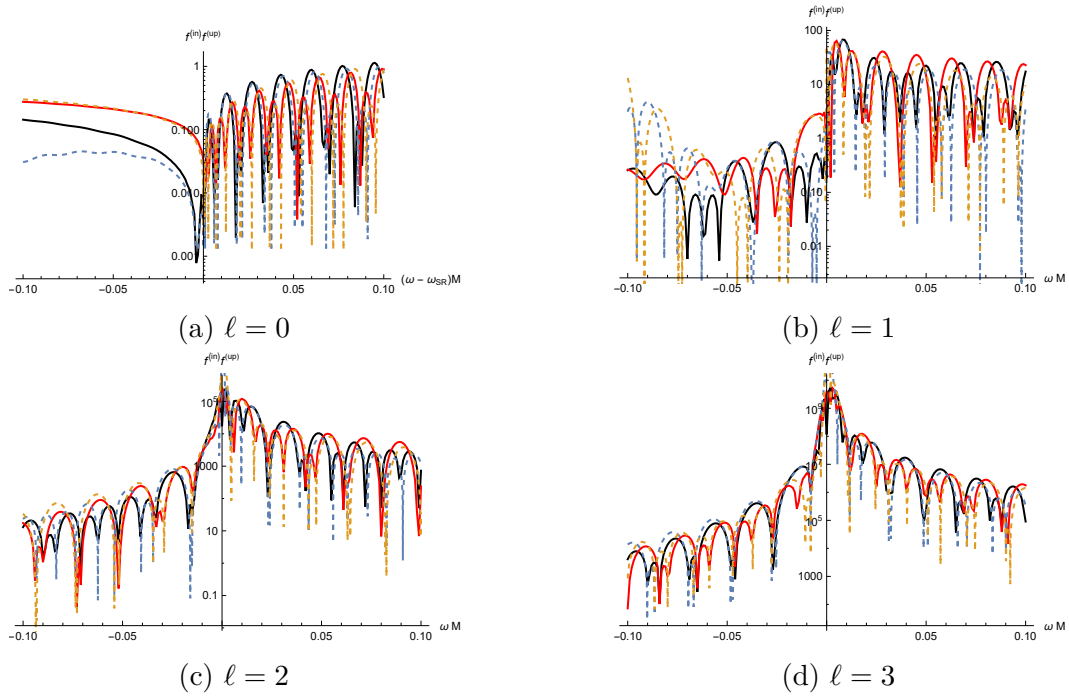


Figure 16 – Log-plots of the real and imaginary parts of  $f_{l\omega}^{(in)} f_{l\omega}^{(up)}$  for different values of  $l$  defined using analytical and numerical solutions, in the approximation of low-frequencies. Black and red are numerical solutions, while blue and orange the analytical ones, being black/blue real and red/orange imaginary parts.

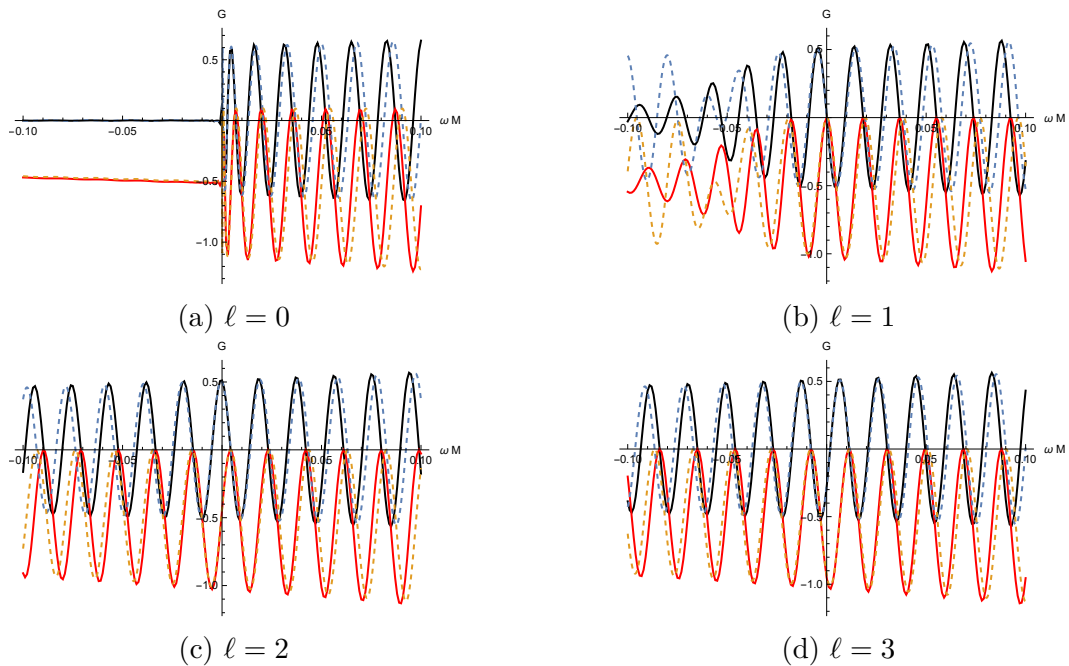


Figure 17 – Plots of the real and imaginary parts of  $G_l$  for different values of  $l$  defined using analytical and numerical solutions in the approximation of low-frequencies. Black and red are numerical solutions, while blue and orange the analytical ones, being black/blue real and red/orange imaginary parts.

### 7.2.1 Numerical

In order to compare with the analytical solutions in the next sections, we will construct the numerical retarded Green function solution for a specific mode ( $\ell = 0$ ) using the expression (4.2). So first we had to calculate  $G_0$  defined in (4.5).

As we said previously, the parameters used are:  $Q = 0.99995M$ ,  $qM = 1$ ,  $r_0 = r_+ + 10^{-3}M$ ,  $\ell = 0$ . We had construct the IN-solutions using (6.14) and UP-solutions according to subsection 6.1.2.

First we solve the ODE numerically to get  $f^{(\text{up})}$  varying  $\omega M$  with 0.01 from  $\omega M \in [-20, 20]$ .

Using it, we get the following plots

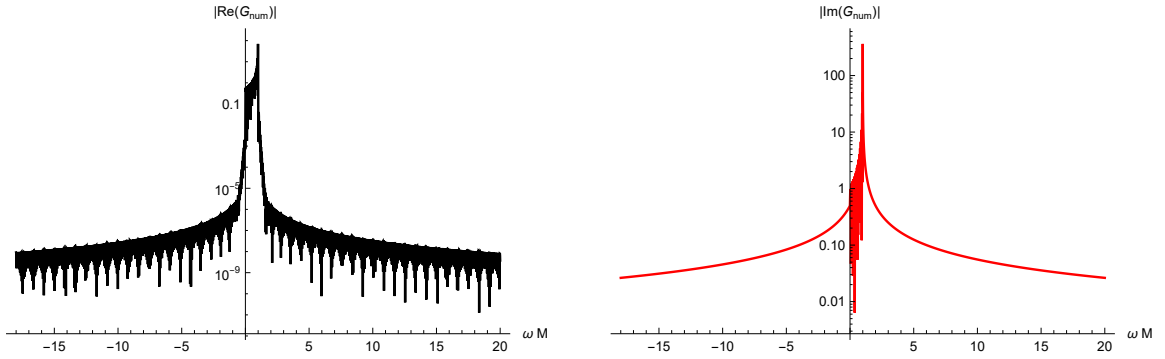


Figure 18 – Log-plots of the real (black) and imaginary (red) parts of  $G_0$ .

what we need to integrate by the following way

$$\mathcal{G}_0^{\text{ret}} = \frac{1}{2\pi r_0^2} \int_{-\infty}^{+\infty} d\omega G_0(r_0, \omega) e^{-i\omega\Delta t}. \quad (7.5)$$

We can see that  $G_0$  when  $\omega M < 0$  and  $\omega M > \omega_{\text{SR}}M$  are in a considerably lower order of magnitude when compared to  $0 < \omega M < \omega_{\text{SR}}M$ .

So, we increase the precision of this function decreasing the stepsize of  $\omega M$  to 0.0001 and now with a total range from  $\omega M \in [-2, 2]$ .

Doing a linear-plot, in Figure (19), it is even more visible the small contribution for higher and lower frequencies.

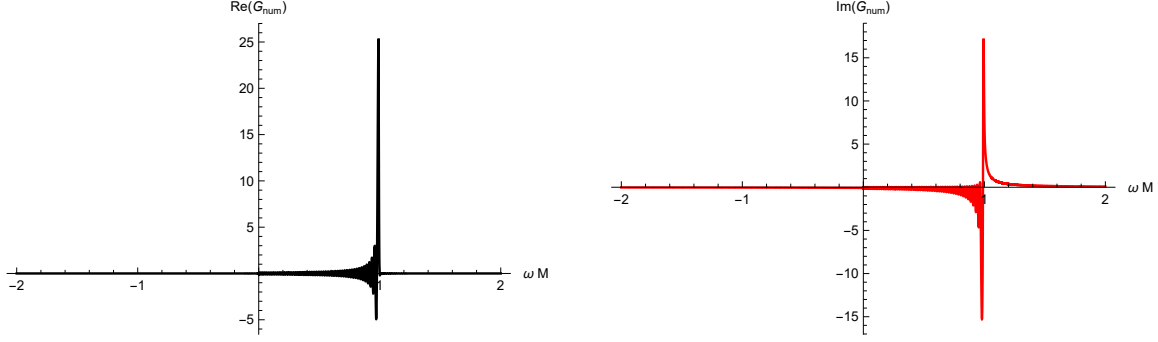


Figure 19 – Plot for the real (black) and imaginary (red) parts of  $G_0$ .

So, taking the real part of  $\mathcal{G}_0^{\text{ret}}$ , using  $\Delta t = t - t'$  where  $t' = 2r_*$  (this choice is made clear in subsection 7.2.2), and integrating in this new range we can write

$$\Re \{ \mathcal{G}_0^{\text{ret}} \} \simeq \frac{1}{2\pi r_0^2} \int_{-2}^{+2} d\omega \Re \{ G_0 \} \cos \omega(t - 2r_*) + \Im \{ G_0 \} \sin \omega(t - 2r_*). \quad (7.6)$$

To be able to do this integral, we use Mathematica. We interpolated  $G_0$ , then numerically integrated its product with the exponential using a PrecisionGoal of 6.

We did it for several times  $t$ , more precisely from  $t/M \in (0, 2000]$  using two different stepsizes. From  $t/M \in (0, 1]$  we use 0.01, while from  $t/M \in (1, 2000]$  we use 0.05.

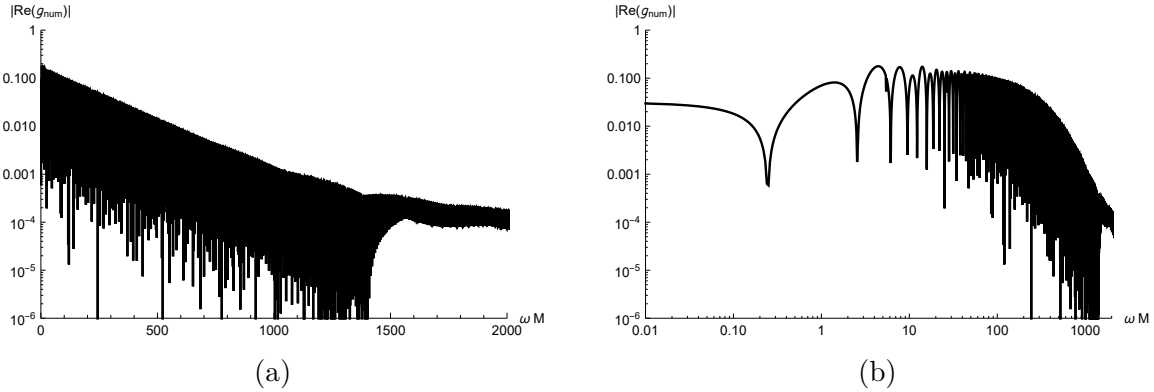


Figure 20 – Log-plot and loglog-plot of real part of  $\mathcal{G}_0^{\text{ret}}$ .

Let's better associate the phases of the graph as we explore analytical solutions.

## 7.2.2 Quasinormal modes

As we discussed in section 4.1, the QN contribution for the retarded GF is described by equation (4.10).

These simple poles are described as QNMs, and have a spectrum defined in (5.46).

But we also need to guarantee that this sum over  $n$  is convergent. As we are using  $r \sim r_+$ , we can use the asymptotic expression  $f_{\ell\omega_{\ell n}}^{(\text{in})} \sim e^{-i\tilde{\omega}_{\ell n}r_*}$  and  $f_{\ell\omega_{\ell n}}^{(\text{up})} \sim B_{\ell,n}^{(\text{in})} e^{-i\tilde{\omega}_{\ell n}r_*}$ , and get,

$$G_\ell^{\text{QN}} \sim \sum_n \frac{e^{-2i\tilde{\omega}_{\ell n}r_*} e^{-i\omega_{\ell n}\Delta t}}{2\omega_{\ell n}\alpha_{\ell n}}, \quad (7.7)$$

where  $\tilde{\omega}_{\ell n} = \omega_{\ell n} - qQ/r_+$ . And knowing that  $\omega_{\ell n} = \Re(\omega_{\ell n}) + i\Im(\omega_{\ell n})$ , we can obtain  $e^{-2i\tilde{\omega}_{\ell n}r_*} e^{-i\omega_{\ell n}\Delta t} = e^{\Im(\omega_{\ell n})T} e^{-2i\Re(\tilde{\omega}_{\ell n})r_* - i\Re(\omega_{\ell n})\Delta t}$  which  $T = \Delta t + 2r_*$ , and finally rearrange  $G_\ell^{\text{QN}}$  as

$$G_\ell^{\text{QN}} \sim \Re \sum_n C_{\ell,n} e^{-2i\Re(\tilde{\omega}_{\ell n})r_* - i\Re(\omega_{\ell n})\Delta t}, \quad (7.8)$$

where

$$C_{\ell,n} = \frac{e^{\Im(\omega_{\ell n})T}}{2\omega_{\ell n}\alpha_{\ell n}}. \quad (7.9)$$

We need to check if this sum is convergent: is essential to take into account the sign of the exponential. We already known that  $\Im(\omega_{\ell n}) < 0$  for every  $n$  and  $\ell$ . But  $T$  could be, at least in principle, positive, negative or even zero.

We will use the d'Alembert's criterion to investigate the convergence. Just remembering, it consist of doing the following:  $\lim_{n \rightarrow +\infty} |C_{\ell,n+1}/C_{\ell,n}| = L$ , if  $L < 1$  we have an absolute convergent series, if  $L > 1$  or  $L \rightarrow 1^+$  it is divergent and if  $L = 1$  or  $L \rightarrow 1^-$  it is inconclusive.

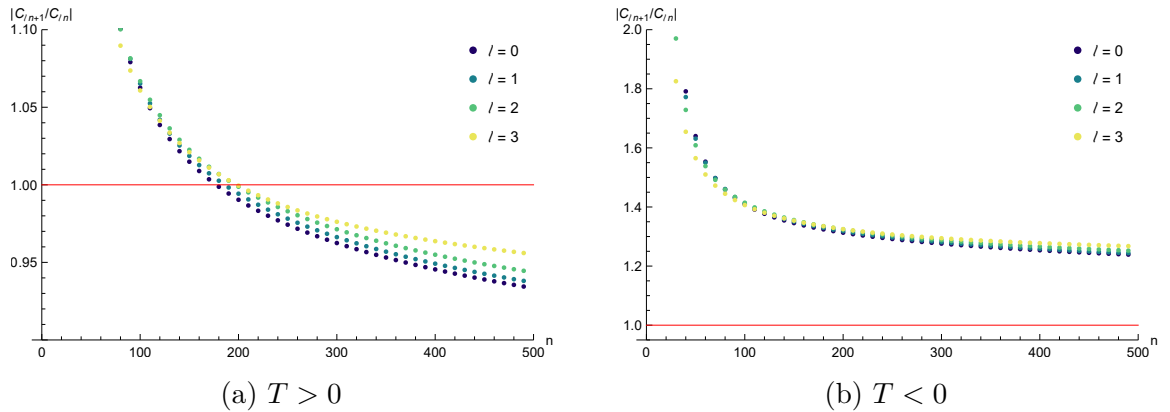


Figure 21 – Plots of  $|C_{\ell,n+1}/C_{\ell,n}|$  using  $T = \pm 10$  for different values of  $\ell$ .

In Figure 21, we can see that only when  $T > 0$  the series is convergent, we can fix this without any problem. As  $\Delta t = t - t'$  we only needs to define  $t' = 2r_*$ , where  $r_* = r_*(r_0)$ .

Having it in mind, we can now take a look for individual modes, and truncate the sum in  $n$  justifying it with the difference of orders of magnitude for the first modes. We are looking for the real part of  $G^{\text{QN}}$ , and this comparison between the modes can be seen in Figure 22.

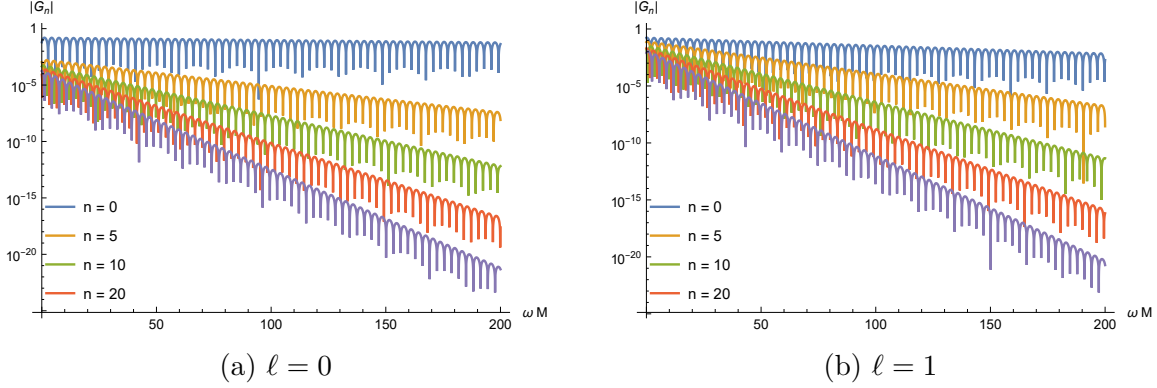


Figure 22 – Log-plots of the real part of  $G_{\ell,n}^{\text{QN}}$

we choose  $n_{\text{cut}} = 20$ .

We can plot  $\mathcal{G}_0^{\text{QN}}$  in the same range as Figure 20.

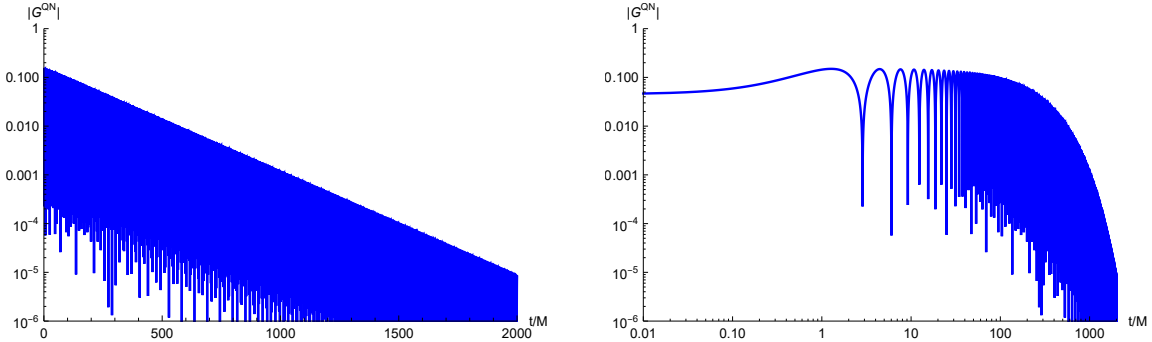


Figure 23 – Log-plot and loglog-plot of  $\mathcal{G}_0^{\text{QN}}$ .

and now we are able to compare with  $\mathcal{G}_0^{\text{ret}}$ .

It is done in Figure 24. For initial times the retarded GF is dominated by the HF-modes, we can see that they contribute very little and quickly, around  $t/M = 15$ , the function is dominated by QNMs. The  $\mathcal{G}_0^{\text{QN}}$  describes correctly  $\mathcal{G}_0^{\text{ret}}$  until around  $t/M \sim 900$ , when an oscillatory tail begins to emerge due to the combination of QNMs and BC (what can be call as “middle-late” time), and will be dampened as time progresses (late-time).

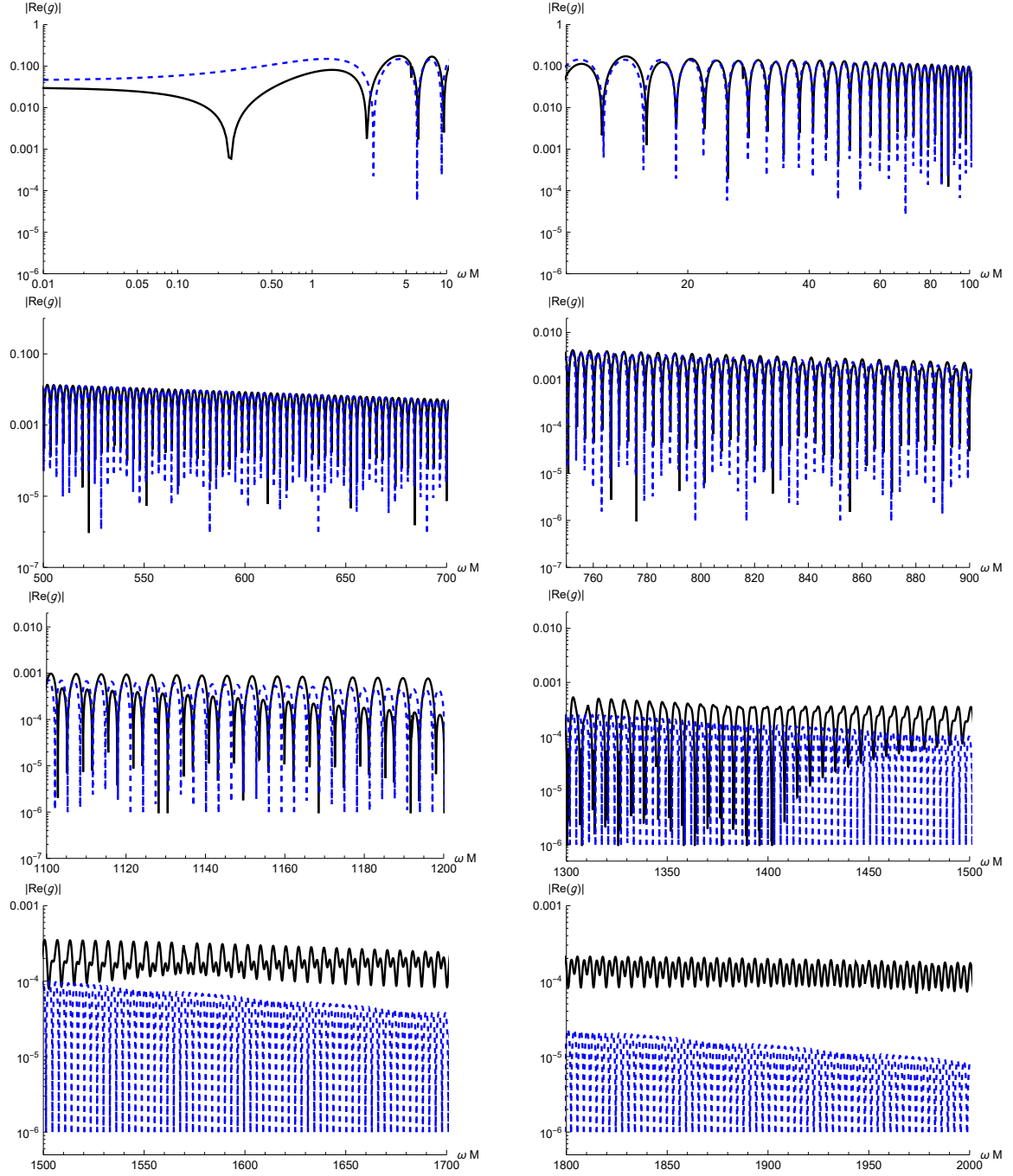


Figure 24 – Log-plot and loglog-plot of numerical  $\mathcal{G}_0^{\text{ret}}$  and  $\mathcal{G}_0^{\text{QN}}$  for several times.

### 7.2.3 Branch-cut

As discussed in section 4.2, the contribution of the BC is described by equation (4.17), where  $\Delta G_\ell$  is given by equation (4.19).

Unfortunately, different from Hod and Andersson [Hod e Piran 1998, Andersson 1997] we were unable to integrate  $\Delta G_\ell$  analytically and find the time power-law dependency due to the complexity of its terms, so we did it numerically as a first approach. In their cases, they are studying far-away field solutions and this leads to crucial differences:

instead a hypergeometric function as solution, they have a confluent hypergeometric function as solution, the same solution that we found in equation (5.22) but they don't make a matching with a near-horizon solution. The wronskian between this confluent hypergeometric function isn't a multi-valuated function, what turns much more easier the equation (4.19).

Looking at Figure 25, we can see that only really low-frequencies will contribute to the integral when the time increase (for small times the GF is dominated by QNMs and HF as we already known), which allows us to use the smaller range from now on.

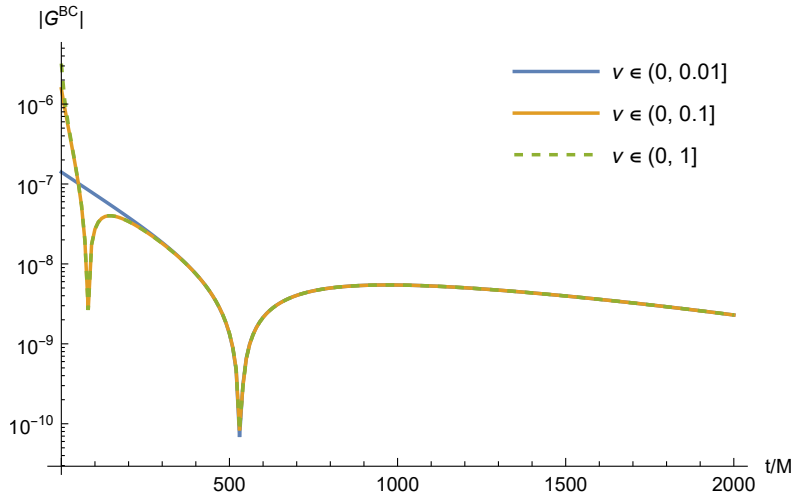


Figure 25 – Log-plot  $G$

We also do not see the oscillations that appear in Figure 20 in the same range because the tail for BC appears with a completely different order of magnitude. These difference may therefore indicate a numerical limitation of our numerical GF, as the steps are on the order of  $10^{-4}$ , the time from  $\sim 10^3$  on may be starting to be problematic or a request of more precision for GF at low frequencies.

So, now we will combine  $G_0^{\text{QN}}$  and  $G_0^{\text{BC}}$  and extend to higher times in Figure 26

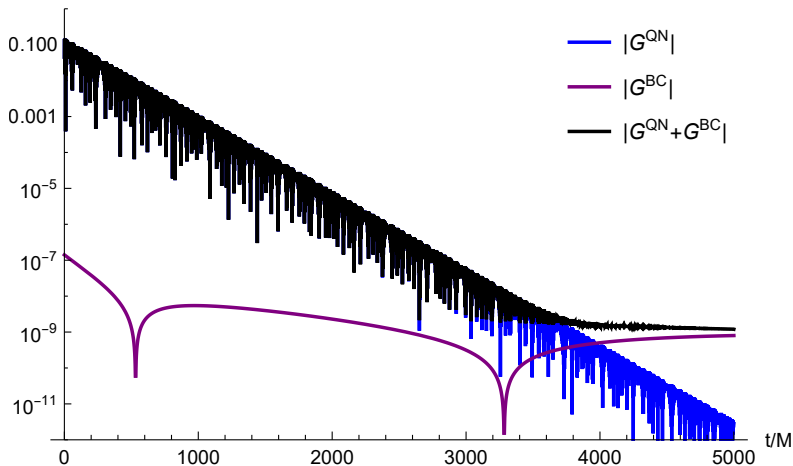


Figure 26 – Log-plot  $G$

## 7.2.4 Retarded Green function

After seeing the agreement between the solutions for  $t/M$  until around 900 so let's continue with our analytical solutions because this miss-match for “middle-late” and late-time was probably due to an issue in the numerical solution.

We can plot  $\mathcal{G}_\ell^{\text{ret}}$  defined by equation (4.2), and sum over  $\ell$ . To do this, is important remember that  $\varphi - \varphi' = \Omega\Delta t$  where  $\Omega = \nu/r_0$ . So, we have, as was shown in chapter 4:

$$G_{\text{ret}}(x, x') = \sum_{\ell=0}^{\infty} \mathcal{G}_\ell^{\text{ret}}, \quad (7.10)$$

$$\mathcal{G}_\ell^{\text{ret}} = \frac{1}{rr'}(2\ell + 1)P_\ell(\cos \Omega\Delta t)G_\ell^{\text{ret}}(r, r', \Delta t), \quad (7.11)$$

Starting with the QNM-solution, we can see the comparison between individual  $\ell$ -modes in Figure 27. Just like to  $n$  we can choose an  $\ell_{\text{cut}}$  and analyzing these plots  $\ell_{\text{cut}} = 10$  is enough.

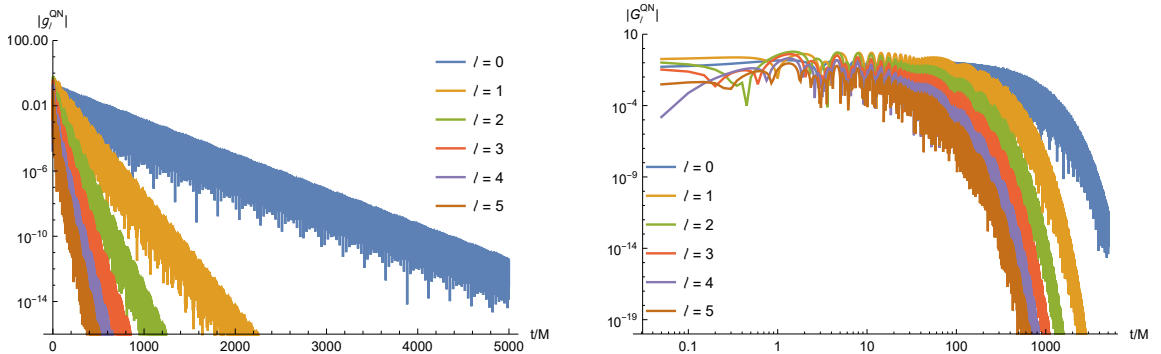


Figure 27 – Log-plot and loglog-plot of individual modes of  $\mathcal{G}_\ell^{\text{QNM}}$ .

Exactly the same can be done to the BC solution, in Figure 28 we compare individual  $\ell$ -modes.

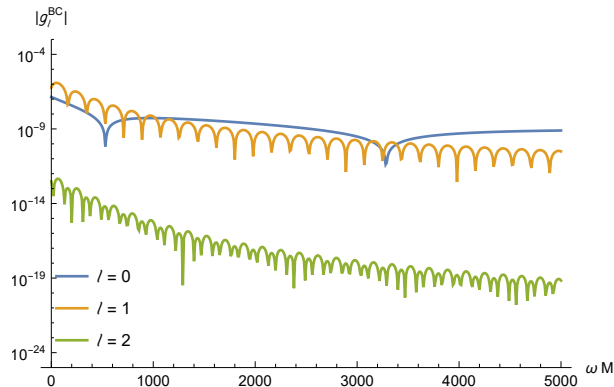


Figure 28 – Loglog-plot of individual modes of  $\mathcal{G}_\ell^{\text{BC}}$ .

Even for  $\ell = 0$  the tail have an slow oscillation. The interference between  $\ell = 0$  and  $\ell = 1$  parts generate an more obvious oscillation that will remains even after the “middle-late” times. In [Koyama e Tomimatsu 2001], Koyama & Tomimatsu showed that for a neutral massive scalar field, if this mass is small, as oscillatory tail emerge with a inverse power-law multiplying a sine of this mass multiplied by time.

And we can sum BC and QN contributions to form a semi-analytical retarded Green function, Figure LAST ONE.

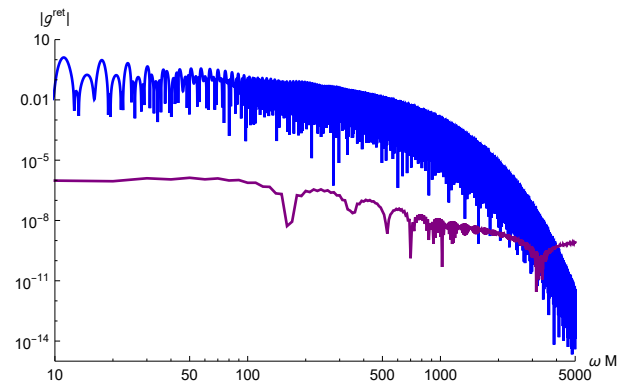


Figure 29 – Loglog-plot of  $|\mathcal{G}^{\text{BC}} + \mathcal{G}^{\text{QN}}|$ .

## 8 Conclusion

We can divide this thesis into two parts, both fundamentally relying on the solutions we obtained valid for near-extremal BH close to the superradiant-bound regime and low-frequencies. Utilizing an exact solution that we also obtained to aid.

The first part consisted of a fully spectroscopic study where we investigated the phenomenon of superradiance through the amplification factor, reobtaining a known result in extremal-Kerr BH [Starobinsky 1974] (here in extremal-RN) and obtained an expression, in this regime, for the near-extremal case. For the QNMs, we recalculated the frequency spectrum ZDM obtained for the first time by Hod [Hod 2010], numerically calculated the DMs [Richartz e Giugno 2014, Cavalcante e Cunha 2021], showed the emergence of the BC for  $Q \rightarrow M$ , and also obtained a numerical formula to calculate these all these QNMs and the TRMs numerically using the confluent Heun function extending the method of Fiziev [Fiziev 2007] to also apply to charged BHs. We also obtained an analytical spectrum of the TRMs which is identical to the case of a scalar field in Kerr spacetime [Casals e Micchi 2019].

The second half consists of developing the Green function, calculated semi-analytically. The part of QNMs is completely analytical, but the integration of Fourier modes for the low-frequency regime needed to be done numerically. We also had a problem comparing our solution for late-times, but we have a strong indication that this was a numerical problem.

Improving this latter part, perhaps by adding some approximation, obtaining the analytical Green function for BC contribution will allow us to write a reasonable analytical solution for the retarded Green function (which is already an interesting result) but also enables us to calculate, for example, the self-force for this particle in this circular orbit that we described.



# Bibliography

- ABBOTT, B. P. et al. Gw150914: The advanced ligo detectors in the era of first discoveries. *Physical review letters*, APS, v. 116, n. 13, p. 131103, 2016. Citado na página 20.
- ANDERSSON, N. Evolving test fields in a black-hole geometry. *Physical Review D*, APS, v. 55, n. 2, p. 468, 1997. Citado na página 69.
- BRITO, R.; CARDOSO, V.; PANI, P. *Superradiance*. [S.l.]: Springer, 2020. v. 10. Citado na página 19.
- CASALS, M. et al. Self-force and green function in schwarzschild spacetime via quasinormal modes and branch cut. *Physical Review D*, APS, v. 88, n. 4, p. 044022, 2013. Citado na página 29.
- CASALS, M.; MICCHI, L. F. L. Spectroscopy of extremal and near-extremal kerr black holes. *Physical Review D*, APS, v. 99, n. 8, p. 084047, 2019. Citado 2 vezes nas páginas 57 and 73.
- CAVALCANTE, J. P.; CUNHA, B. C. da. Scalar and dirac perturbations of the reissner-nordström black hole and painlevé transcendentals. *Physical Review D*, APS, v. 104, n. 12, p. 124040, 2021. Citado 2 vezes nas páginas 57 and 73.
- CHANDRASEKHAR, S. *The mathematical theory of black holes*. [S.l.]: Oxford university press, 1998. v. 69. Citado na página 19.
- CHRISTODOULOU, D. Reversible and irreversible transformations in black-hole physics. *Physical Review Letters*, APS, v. 25, n. 22, p. 1596, 1970. Citado na página 19.
- FIZIEV, P. P. Exact solutions of regge-wheeler equation. In: IOP PUBLISHING. *Journal of Physics: Conference Series*. [S.l.], 2007. v. 66, n. 1, p. 012016. Citado 2 vezes nas páginas 51 and 73.
- HOD, S. Relaxation dynamics of charged gravitational collapse. *Physics Letters A*, Elsevier, v. 374, n. 29, p. 2901–2903, 2010. Citado 3 vezes nas páginas 20, 57, and 73.
- HOD, S.; PIRAN, T. Late-time evolution of charged gravitational collapse and decay of charged scalar hair. ii. *Physical Review D*, APS, v. 58, n. 2, p. 024018, 1998. Citado na página 69.
- ISRAEL, W. Event horizons in static vacuum space-times. *Physical review*, APS, v. 164, n. 5, p. 1776, 1967. Citado na página 26.
- ISRAEL, W. Event horizons in static electrovac space-times. *Communications in Mathematical Physics*, Springer, v. 8, p. 245–260, 1968. Citado na página 26.
- KOYAMA, H.; TOMIMATSU, A. Asymptotic power-law tails of massive scalar fields in a reissner-nordström background. *Physical Review D*, APS, v. 63, n. 6, p. 064032, 2001. Citado na página 72.

MENZA, L. D.; NICOLAS, J.-P. Superradiance on the reissner–nordström metric. *Classical and Quantum Gravity*, IOP Publishing, v. 32, n. 14, p. 145013, 2015. Citado na página 19.

MOTYGIN, O. V. On evaluation of the confluent heun functions. In: IEEE. *2018 Days on Diffraction (DD)*. [S.l.], 2018. p. 223–229. Citado na página 51.

PENROSE, R. Gravitational collapse: The role of general relativity. *Nuovo Cimento Rivista Serie*, v. 1, p. 252, 1969. Citado na página 19.

PRESS, W. H.; TEUKOLSKY, S. A. Floating orbits, superradiant scattering and the black-hole bomb. *Nature*, Nature Publishing Group UK London, v. 238, n. 5361, p. 211–212, 1972. Citado na página 19.

PRESS, W. H.; TEUKOLSKY, S. A. Perturbations of a rotating black hole. ii. dynamical stability of the kerr metric. *Astrophysical Journal*, Vol. 185, pp. 649-674 (1973), v. 185, p. 649–674, 1973. Citado na página 19.

PUGLIESE, D.; QUEVEDO, H.; RUFFINI, R. Circular motion of neutral test particles in reissner-nordström spacetime. *Physical Review D*, APS, v. 83, n. 2, p. 024021, 2011. Citado na página 33.

PUGLIESE, D.; QUEVEDO, H.; RUFFINI, R. Motion of charged test particles in reissner-nordström spacetime. *Physical Review D*, APS, v. 83, n. 10, p. 104052, 2011. Citado na página 33.

REGGE, T.; WHEELER, J. A. Stability of a schwarzschild singularity. *Physical Review*, APS, v. 108, n. 4, p. 1063, 1957. Citado na página 19.

RICHARTZ, M. Quasinormal modes of extremal black holes. *Physical Review D*, APS, v. 93, n. 6, p. 064062, 2016. Citado na página 57.

RICHARTZ, M.; GIUGNO, D. Quasinormal modes of charged fields around a reissner-nordström black hole. *Physical Review D*, APS, v. 90, n. 12, p. 124011, 2014. Citado 2 vezes nas páginas 57 and 73.

RUFFINI, R.; WHEELER, J. A. Introducing the black hole. *Physics today*, American Institute of Physics, v. 24, n. 1, p. 30–41, 1971. Citado na página 26.

STAROBINSKY, A. Amplification of waves reflected from kerr black holes. In: CAMBRIDGE UNIVERSITY PRESS. *Symposium-International Astronomical Union*. [S.l.], 1974. v. 64, p. 94–94. Citado 2 vezes nas páginas 55 and 73.

TEUKOLSKY, S. A. Perturbations of a rotating black hole. i. fundamental equations for gravitational, electromagnetic, and neutrino-field perturbations. *Astrophysical Journal*, Vol. 185, pp. 635-648 (1973), v. 185, p. 635–648, 1973. Citado na página 19.

TEUKOLSKY, S. A.; PRESS, W. H. Perturbations of a rotating black hole. iii-interaction of the hole with gravitational and electromagnetic radiation. *Astrophysical Journal*, vol. 193, Oct. 15, 1974, pt. 1, p. 443-461., v. 193, p. 443–461, 1974. Citado na página 19.

VISHVESHWARA, C. Scattering of gravitational radiation by a schwarzschild black-hole. *Nature*, Nature Publishing Group UK London, v. 227, n. 5261, p. 936–938, 1970. Citado na página 20.

ZEL'DOVICH, Y. B. Generation of waves by a rotating body. *Soviet Journal of Experimental and Theoretical Physics Letters*, v. 14, p. 180, 1971. Citado na página 19.